AGU PUBLICATIONS

Geochemistry, Geophysics, Geosystems

RESEARCH ARTICLE
10.1002/2014GC005485

Key Points:
- Two wide-angle seismic profiles crossing the Rif Cordillera are described
- Significant lateral variations in the Moho

Supporting Information:
- Readme
- Figures S1 and S2

Correspondence to:
A. Gil,
agil@ictja.csic.es

Citation:
Gil, A., J. Gallart, J. Diaz, R. Carbonell, M. Torne, A. Levander, and M. Harnafi (2014), Crustal structure beneath the Rif Cordillera, North Morocco, from the RIFSIS wide-angle reflection seismic experiment, *Geochem. Geophys. Geosyst.*, *15*, 4712–4733, doi:10.1002/2014GC005485.

Received 7 JUL 2014
Accepted 6 NOV 2014
Accepted article online 11 NOV 2014
Published online 9 DEC 2014

Crustal structure beneath the Rif Cordillera, North Morocco, from the RIFSIS wide-angle reflection seismic experiment

Alba Gil[1], Josep Gallart[1], Jordi Diaz[1], Ramon Carbonell[1], Montserrat Torne[1], Alan Levander[2], and Mimoun Harnafi[3]

[1]Department of Earth Structure and Dynamics, Institute of Earth Sciences Jaume Almera-CSIC, Barcelona, Spain, [2]Department of Earth Sciences, Rice University, Houston, Texas, USA, [3]Institut Scientifique, Université Mohammed V-Agdal, Rabat, Morocco

Abstract The different geodynamic models proposed since the late 1990s to account for the complex evolution of the Gibraltar Arc System lack definite constraints on the crustal structure of the Rif orogen. Here we present the first well-resolved P-wave velocity crustal models of the Rif Cordillera and its southern continuation toward the Atlas made using controlled-source seismic data. Two 300+ km-long wide-angle reflection profiles crossed the Rif along NS and EW trends. The profiles recorded simultaneously five land explosions of 1Tn each using ~850 high frequency seismometers. The crustal structure revealed from 2-D forward modeling delineates a complex, laterally varying crustal structure below the Rif domains. The most surprising feature, seen on both profiles, is a ~50 km deep crustal root localized beneath the External Rif. To the east, the crust thins rapidly by 20 km across the Nekkor fault, indicating that the fault is a crustal scale feature. On the NS profile the crust thins more gradually to 40 km thickness beneath Middle Atlas and 42 km beneath the Betics. These new seismic results are in overall agreement with regional trends of Bouguer gravity and are consistent with recent receiver function estimates of crustal thickness. The complex crustal structure of the Rif orogen in the Gibraltar Arc is a consequence of the Miocene collision between the Iberian and African plates. Both the abrupt change in crustal thickness at the Nekkor fault and the unexpectedly deep Rif crustal root can be attributed to interaction of the subducting Alboran slab with the North African passive margin at late Oligocene-early Miocene times.

1. Introduction

At the westernmost Mediterranean the complex interactions between two continental masses, the Eurasian and African plates, has produced a broad arcuate collision zone, the Gibraltar Arc System (Figure 1), composed of the Betic and Rif mountain ranges separated by the Alboran Sea basin. A wide variety of tectonic models have been proposed, to explain the surface geology [see *Platt et al*., 2013 for a review] whereas only recently has detailed information been available of the deep structure of much of this region, including the Rif Cordillera in North Morocco.

Crustal thicknesses, composition, structure, and the location of major fault zones reflect deformation processes, which is fundamental knowledge necessary to constrain evolutionary models. Over 100 years after its discovery the depth of the Mohorovicic discontinuity is still poorly known in many geodynamically complex areas [see *Carbonell et al*., 2013 for a review]. The Gibraltar Arc System is one such area. *Diaz and Gallart* [2009] and *Gallart and Diaz* [2013] reported the crustal thickness measurements presently available in the Iberian Peninsula, revealing that the northern part of this complex collision zone features crustal thicknesses between 30 and 43 km, the latter found beneath specific areas of the Betic ranges. However, recent receiver function analyses suggest greater crustal thicknesses in parts of the Betics and in the Moroccan Rif. Here we present an analysis of wide-angle seismic data which allows the development of a velocity-depth model of the crust and hence provide new insights on the Moho topography beneath the area.

Numerous, often incompatible geodynamic models have been proposed to explain the singular configuration of the Gibraltar Arc System. They include: regional-scale recycling of the lithosphere by delamination [*Seber et al*., 1996]; slab break-off [*Blanco and Spakman*, 1993; *Zeck*, 1996], convective removal [*Platt and Vissers*, 1989]; active eastward subduction of oceanic crust [*Gutscher et al*., 2002]. Further details on those

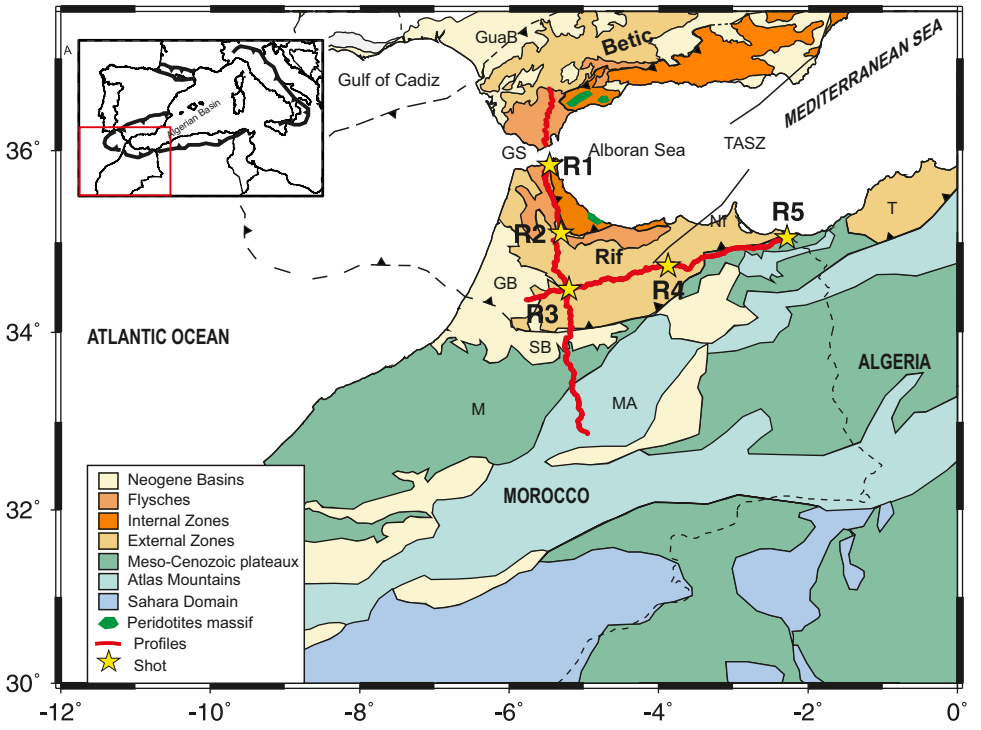

Figure 1. Map of Southern Iberia and Northern Morocco with the location of seismic wide-angle profiles acquired through the RIFSIS project (in red, the digital stations; stars, the source points) and simplified geology of the study area. The major tectonic domains and boundaries are indicated. GB: Gharb Basin; GuaB: Guadalquivir Basin; GS: Gibraltar Strait; M: Meseta; MA: Middle Atlas; Nf: Nekkor fault; SB: Saïss Basin; T: Tell Mountain TASZ: Trans-Alboran Shear Zone. The dashed line represents the geometry of the Gibraltar Arc. The inset shows location within the Euro-Mediterranean domain and includes an outline of the Westernmost Mediterranean Alpine Belt.

models, including a summary diagram, can be found at the review paper presented by *Platt et al*. [2013]. Many authors now relate the origin of the Gibraltar Arc to the segmentation of the Western Mediterranean Subduction Zone (WMSZ) and the fast westward oriented retreat of the subsequent narrow slab of oceanic lithosphere [*Royden*, 1993; *Lonergan and White*, 1997; *Rosenbaum and Lister*, 2004; *Faccenna et al*., 2004; *Jolivet et al*., 2009; *Vergés and Fernàndez*, 2012]. Recent mantle studies of this region suggest subduction related convective recycling and delamination of mantle lithosphere from the crust [*Bezada et al*., 2013; *Palomeras et al*., 2014; *Thurner et al*., 2014]. The crustal models presented here helped constrain these recent studies by providing a detailed knowledge of the crustal properties.

With an aim to improving the constraint on geodynamic models of the Gibraltar Arc, an ambitious multidisciplinary research project was initiated in 2006, led by the Spanish Topo-Iberia program in collaboration with PICASSO (Program to Investigate Convective Alboran Sea System Overturn), a loosely affiliated consortium of U.S., Irish, German and Moroccan institutions. Within these initiatives special emphasis was placed on geophysical characterization of the crust with active seismic and magnetotelluric methods in specific areas coinciding with surface structural and petrological studies. These extended from the center of the Iberian Peninsula [*Gómez-Ortiz et al*., 2011; *Pous et al*., 2011; *Martínez-Poyatos et al*., 2012; *Ruiz-Constán et al*., 2012; *Ehsan et al*., 2014; *García-Lobón et al*., 2014] to the Saharan craton, south of the Atlas Mountains. A unique high resolution wide-angle reflection data set was acquired across the Atlas [*Ayarza et al*., 2014] and across the Rif (this manuscript).

We present seismic crustal velocity models along a 430 km-long and a 330 km-long wide-angle seismic reflection (WA) transects crossing the Rif in the NS and EW directions. This geometry is aimed to acquire seismic data over the zone where a significant low Bouguer anomaly has been previously identified [*Hildengrand et al*., 1998]. The Bouguer gravity anomaly database maintained by the International Gravimetric Bureau (BGI; http://bgi.omp.obs-mip.fr/data-products/Grids-and-models/wgm2012) shows a very prominent −150 mGal gravity low is located to the south of the Internal Zones of the Rif, over the External Zones and the western region of the Gharb foredeep basin (Figure 2). The gravity anomaly increases toward the

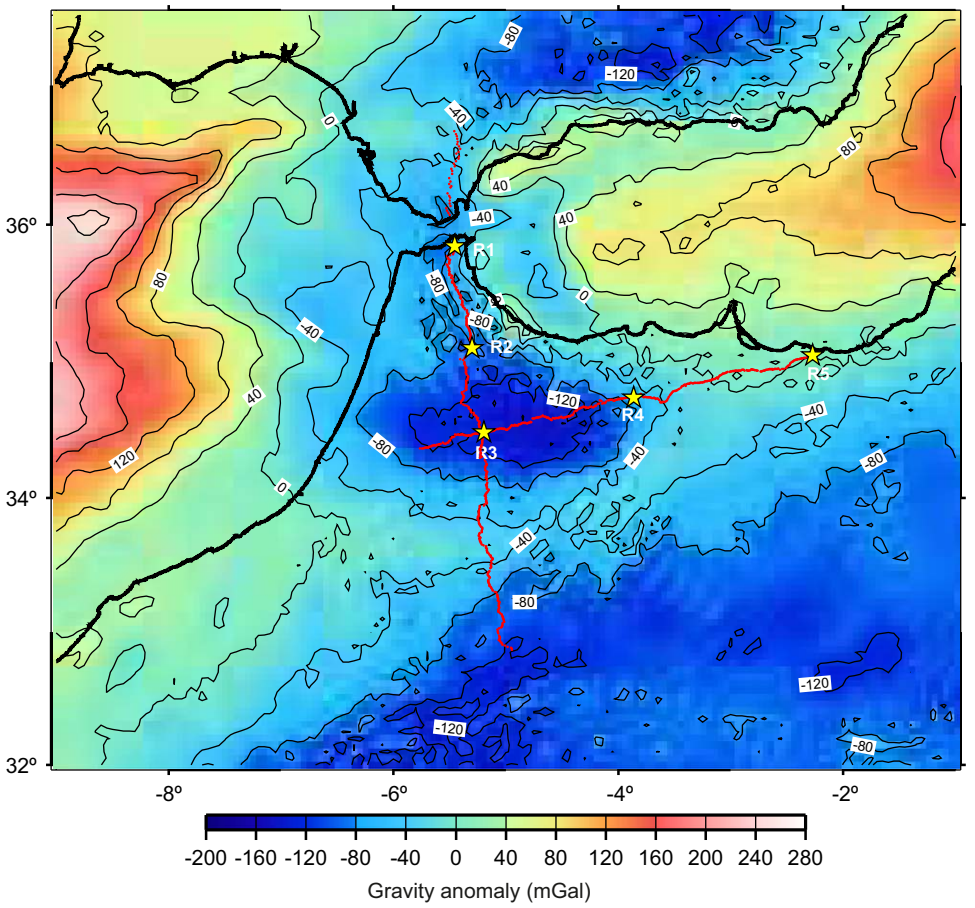

Figure 2. Gravity anomaly contour map of the southern Iberian Peninsula and northern Morocco. Bouguer anomalies have been extracted from the BGI (Bureau Gravimétrique International, http://bgi.obs-mip.fr). The contour interval is 40 mGal. The red lines indicate the location of the seismic profiles and the yellow stars represent the source points. Note that the wide-angle transects closely follow the axes of the minimum of the Bouguer anomaly (−150 mGal) beneath the Rif domain.

oceanic areas, reaching maximum values of up to 250 mGal over the Atlantic and from 50 to 150 mGal in the Alboran Basin and its transition toward the oceanic Algerian basin (Figures 1 and 2). The new seismic models derived from our data are converted to density and the predicted Bouguer anomaly is compared with the BGI database.

2. Geological Setting

The Gibraltar Arc system forms the Westernmost Mediterranean Alpine belt and comprises the Betic and Rif Cordilleras and a deep sedimentary basin over the extended continental crust of the Alboran Sea, which developed roughly synchronously with the orogenic belt during the Miocene [*Vergés and Fernàndez*, 2012; *Platt et al*., 2013].

Similar to the Betic Ranges and other Alpine Mediterranean cordilleras, the Rif consists of Internal and External Zones, separated by Flysch units. The Internal zones are formed by Paleozoic, Mesozoic and Cenozoic sequences, including metamorphic complexes that have been affected by Alpine deformation since the Eocene-Late Oligocene [*Chalouan et al*., 2001, 2008]. The External Zones comprise carbonate and pelitic Mesozoic and Cenozoic units, mainly limestone and marls. In the Rif, they form a fold-and-thrust belt detached along Late Triassic evaporite beds above the thinned continental crust of the North Africa passive margin [*Wildi*, 1983; *Chalouan et al*., 2008]. The Flysch units are composed of Cretaceous-Lower Miocene detrital rocks. They overthrust the External Rif units and include klippes located on the Internal Zones [*Chalouan et al*., 1995, 2008]. The relatively large Ronda and Beni-Bousera peridotite exposures (Figure 1) are found along the eastern flank of the Gibraltar Arc in the Betics and the Rif, respectively.

The Gharb (or Rharb) Basin is a foredeep separating the Rif belt from the Moroccan Meseta and Middle Atlas. This basin contains part of the Prerif nappe underlying a large amount of continental sediments, reaching a maximum depth of 8 km toward the west [*Hafid et al*., 2008]. It was moreover filled with sediments of marine origin during the Tertiary and continental formations during the Quaternary, except for a coastal fringe [*Hafid et al*., 2008]. The Gharb Basin, like its counterpart in the Iberian Peninsula, the Guadalquivir Basin, evolved as a foreland basin as the basement was loaded by the thrust sheets of the External Units [*Fernàndez et al*., 1998; *Garcia-Castellanos*, 2002] during the Miocene.

In Early-Middle Miocene, after crustal thickening and metamorphism, the region began to undergo EW to NE-SW extension that thinned the continental crust along normal faults forming the Alboran Basin [*Chalouan et al*., 2008]. The Alboran Basin has thick Neogene overlying deep crustal rocks locally recognized as belonging to the Sebtides-Alpujarride nappes.

Since the Late Miocene, continued compression has formed large folds and reverse faults in the mountain front, as well as normal faults in the upper crustal levels of the Internal Zones, providing the relief of the modern Rif. Large strike-slip faults, notably the Trans-Alboran Shear Zone (TASZ), and its onshore continuation, the Nekkor fault, accommodate escape of Central Rif toward the SW [*Pérouse et al*., 2010]. The TASZ is a broad fault zone, composed of different left-lateral strike-slip fault segments running from the eastern Betics to the Alhoceima region in the Rif and resulting in a major bathymetric high in the Alboran Sea, that affects the Neogene basins of the region [*Udías and Buforn*, 1992; *Martínez-Díaz et al*., 2001]. The Nekkor fault is linked to the normal faults beneath Alhoceimas region [*Booth-Rea et al*., 2012], which is one of the most seismic active areas nowadays in Morocco. More detailed descriptions of the geology of the Gibraltar Arc can be found elsewhere [e.g., *Chalouan et al*., 2008; *Platt et al*., 2013, and references therein].

3. Previous Geophysical Studies

Early geophysical studies of the Rif in the 70's consisting of low-density seismic refraction by *Hatzfeld and Bensari* [1977] reported a crustal thickness of 30 km beneath the Gharb Basin. Beneath the Alboran Sea, wide-angle profiles (also in the 70's) constrain Moho-depths of 18–20 km beneath the central part of the basin [*Working Group for Deep Seismic Sounding in Alboran 1974*, 1978]. *Wigger et al*. [1992] report crustal thicknesses of 35 km beneath the southernmost Rif determined by refraction recordings of quarry blasts.

Torne et al. [2000] used gravity, heat flow and elevation data to estimate crust and mantle lithosphere thickness beneath the Alboran basin, the Betics and the Rif Cordilleras. They found that crustal thickness between the orogenic belts and the Alboran Sea may differ as much as 25 km. These models where further refined by including constraints from the Geoid anomalies [*Frizon de Lamotte et al*., 2004; *Zeyen et al*., 2005] and possible petrological compositions [*Fullea et al*., 2010, 2014]. These resulted in a moderately thick crust underneath the Rif and Betics (∼32–34 km), and a thin continental crust (∼18–22 km) beneath the Alboran basin. This basin progressively thins toward the east, reaching values less than 16 km depth at the transition to the Algerian basin. In the Moroccan interior, crustal thickness increases to 38 km below the highest elevations of the High Atlas, then it decreases to the southeast to 30–32 km.

Results from a NW-SE oriented magnetotelluric profile across the Rif [*Anahnah et al*., 2011a] show a heterogeneous upper crust, with resistive (metamorphic rocks) and conductive (peridotites) bodies in the uppermost 10 km of the Internal Zones, and highly conductive bodies in the External Zones and foreland basin. The variable thicknesses of the latter ones suggest the presence of basement highs that may be related to blind frontal thrusts between the Gharb Basin and the External Zones. A crustal detachment level separating shallow geological units from a probable Variscan basement was inferred. At depths below 5 km, relatively large resistive bodies appear below the frontal part of the Rif. The southern Rif has also been modeled using magnetotelluric data, featuring wide and thin conductive bodies interpreted to correspond to detrital rocks that alternate with marl and carbonates [*Anahnah et al*., 2011b].

Eurasian convergence relative to Africa trended south during the Late Cretaceous-Paleogene, and has trended southeast oblique to the African margin from the Miocene. The present-day tectonic motions in the study area are constrained from GPS observations on permanent sites and temporary deployments [*Fadil et al*., 2006; *Vernant et al*., 2010; *Koulali et al*., 2011] combined with other stress indicators [*Palano et al*., 2013]. They show south to southeast motion at ∼5 mm/yr of the Rif region relative to stable Nubia.

The Rif, Betics and Alboran Sea are an active seismic zone, with the Rif interpreted as a wide transpressive zone between the seismically active Tell to the east, and the oceanic transform fault plate boundary to the west. This is interpreted as additional evidence of subduction roll-back, corresponding to the contact area between two converging plates, Eurasia and Africa.

Local earthquake travel time tomography using data from the TopoIberia and PICASSO arrays of the Gibraltar Arc (L. El Moudnib et al., Crust structure of northern Morocco and southern Iberian Peninsula from local earthquake tomography, submitted to *Tectonophysics*, 2014) have significantly enhanced the previous models presented by *Gurría and Mezcua* [2000] and *Calvert et al*. [2000a]. At the uppermost crustal levels low velocities (5.5–5.75 km/s) are observed beneath the Betics and the Alhoceima region, while the velocities beneath the Rif remain close to the 1-D IGN reference model [*Gurría and Mezcua*, 2000]. At ∼30 km depth, a low velocity zone (6.3–6.7 km/s) clearly underlies the Gibraltar Arc from the easternmost Betics to the southeastern Rif, were an abrupt change in velocity is observed. Low shear velocities have been determined in the same region from Rayleigh wave tomography [*Palomeras et al*., 2014]. *Calvert et al*. [2000b] and *Serrano et al*. [2005] used seismic regional waveforms to map Pn velocities along the Africa-Iberia boundary. A robust low-Pn ($<$7.8 kms^{-1}) velocity anomaly is imaged beneath the Betics, in contrast with the relatively normal values beneath the Alboran Sea. The Rif and Middle Atlas show also low Pn velocities. *Diaz et al*. [2013] resolved similar patterns and a local area of high Pn and Sn velocity ($>$8.2 kms^{-1} and $>$4.8 kms^{-1}, respectively) beneath the Alhoceima region (approx. 35°N, 3°W).

Regional 3-D teleseismic tomography [*Bezada et al*., 2013] images a high velocity slab-like feature beneath the Alboran Sea and much of the eastern Betics from lithospheric depths to $>$600 km. The geometry confirms slab tearing beneath the eastern Betics, suggested previously by *Spakman and Wortel* [2004] and *Garcia-Castellanos and Villaseñor* [2011]. Rayleigh wave tomography and receiver function images of the Western Mediterranean [*Palomeras et al*., 2014; *Thurner et al*., 2014] suggest that the slab is attached to the crust beneath the Rif Cordillera, suggested also by *Pérouse et al*. [2010] from GPS observations.

SKS split directions rotate around the Gibraltar Arc with the fast directions following the curvature of the Rif-Betic chain [*Buontempo et al*., 2008; *Diaz et al*., 2010; *Miller et al*., 2013; *Diaz and Gallart*, 2014].This is interpreted as evidence of asthenospheric mantle flow around the Alboran slab [*Diaz et al*., 2010; *Alpert et al*., 2013; *Diaz and Gallart*, 2014]. Recent Topo-Iberia and PICASSO receiver function studies [*Mancilla et al*., 2012; *Thurner et al*., 2014] show large variations in crustal thickness beneath northern Morocco, with a clearly defined localized crustal root beneath the central Rif extending to 40–50 km, and significantly thinner crustal thicknesses of 22–30 km beneath northeastern Morocco, although the studies differ in detail. The eastern limit of the Rif Cordillera, in the transition between both areas, shows complex converted Ps signals admitting different interpretations. *Thurner et al*. [2014] identified a subcrustal horizon beneath the Betic and Rif Cordilleras, located between 45 and 80 km depth, which are interpreted as the top of the Alboran Sea slab merging with the Moho at 50–55 km depth.

4. RIFSIS Data Acquisition and Processing

In October 2011, we acquired a 330 km-long and a 430 km-long wide-angle seismic reflection profiles oriented, approximately, EW and NS (Figure 1). The profile directions were designed to approximate the overall Rif strike and dip directions and conform to major and minor axes of the elliptical Bouguer anomaly pattern (Figure 2). The EW transect extends across the Rif orogen from the Gharb Basin to the Algerian border. The NS line extended 70 km into the Iberian Peninsula and over 300 km within Morocco to the Mid-Atlas, overlapping with the SIMA seismic wide-angle transect in the Atlas Mountains [*Ayarza et al*., 2014]. Jointly, SIMA and the NS RIFSIS profile extend 700 km-long from the northern Sahara desert into southernmost Iberia. The Iberian portion of the NS RIFSIS profile is not reversed as there were no source points in Iberia.

Each of the 5 sources consisted of 1Tn of chemical explosives in 2 boreholes and was recorded by 845 digital seismographs with one-component 4.5 Hz geophones (Reftek RF125 IRIS-PASSCAL Texans). The average receiver spacing was 750 m. Shots R1 through R3 where located along the NS line, and R3–R5 were along the EW line. Shot R3 is at the intersection of the two profiles. All shots were recorded by all the stations producing fan shots for 3-D control on deep structure [*Carbonell et al*., 2014]. Up to 402 seismographs were deployed along the EW profile and 443 along the NS profile including 35 in Spain. The signal-to-noise ratio

in our data is within the usual range for this kind of experiments, providing a reasonably good overall data quality although shot R1 near Gibraltar has low signal-to-noise ratio at offsets larger than 80 km.

Data processing included amplitude recovery, frequency filtering using a classical band-pass Butterworth filter (3–10 Hz) and phase enhancement by a lateral phase coherency filter [*Schimmel and Gallart*, 2007]. This latter procedure allows a better identification of weak seismic arrivals at large offsets, as can be observed in the supporting information Figure S1. Travel times of different seismic phases were picked for a series of crustal phases including the Moho reflection *PmP*. The coherency filter was especially valuable in the case of shot R1 allowing us to identify arrivals from 80 to 140 km offsets. A total of 2297 picks were obtained, 1154 from the NS profile and 1143 from the EW.

P-wave velocity-depth models were derived by forward modeling travel times of diving and reflected waves using RAYINVR software [*Zelt and Smith*, 1992]. Additional geological and geophysical constraints were considered in the modeling procedure where available. For the NS profile we start from the velocity-depth model presented by *Ayarza et al*. [2014] from the interpretation of the SIMA profile, crossing the Atlas and partially overlapping our profile. At the northern edge, the seismic models by *Medialdea et al*. [1986] were also taken into consideration. Different geological results compiled in *Chalouan et al*. [2008] have been used to get an initial estimation of the geometry and velocities in the uppermost sedimentary layers. Identified seismic phases (shown and labeled in the figures) follow the conventional nomenclature: *Ps* and *Pg* denote refractions through the sedimentary cover and the basement, respectively; *PiP*, *PcP* and *PmP* stand for P to P reflections produced at the top of the middle crust, top of the lower crust and Moho discontinuity, respectively; and *P1*, *P1P* identify refraction and reflection events on a locally limited sedimentary layer. Because the shot spacing is rather large, varying from about 80 to 140 km, phases from the sedimentary layers and the upper crust generally are not reversed, whereas the deeper phases *Pg*, *PcP*, and *PmP* generally are. Despite careful inspection and analysis of the filtered and unfiltered record sections, we have not found clear evidences of arrivals displaying a convincing lateral correlation and which could be attributed to lower crustal or Moho refracted phases. Hence, we have preferred to use only the well identified reflected phases as the observations for modeling. In the following sections we describe: (1) the quality of the data; (2) the parts of the models that are well constrained; and (3) the travel time picks and fit (supporting information Figure S2). Estimated uncertainties of the travel times picks are, on average 0.05 s for *Ps*, 0.1 s for *Pg* and between 0.1 and 0.2 s for reflected phases *PiP*, *PcP* and *PmP*. The derived P-wave velocity models reproduce the picked travel time branches with a very good agreement. The observed travel time misfits (usually less than 0.15 s) are reasonable in view of contributing factors such as the acquisition geometry, local oscillations on topography, outcropping lithologies, etc.

5. Lateral Variations of the Structure Beneath the External Rif Domain: East-West Profile From Gharb Basin to the Algerian Border

The EW profile is sampled from shot records R3, R4 and R5 (Figures 3–5). Rapid structural variations beneath the External Rif domain can be inferred from the deeper phases *PcP* and *PmP* recorded along this transect.

Shot R3 was recorded ~50 km to the west, toward the Gharb Basin, and 280 km to the east, along the External Rif to the Algerian border. Two sedimentary arrivals are observed in the eastern section: Ps_1 is the first arrival to ~15 km and Ps_2, to ~30 km offset. A satisfactory fit in travel times is obtained (see Figure 6) with a velocity gradient between 3.2 and 3.8 km/s for the first sedimentary layer, and 4.25 to 5.2 km/s for the second. In the western part, the first arrival to 15 km offset (−15 km in Figure 3), identified as the refracted phase *P1*, arrives earlier than the same arrival at similar offsets to the east. This *P1* phase, a first arrival to 40 km offset, travels in a layer with an average velocity of 4.8 km/s. This phase and its associated reflection *P1P* indicate that the Neogene deposits of the Gharb Basin extend to depths of 10 km. The *Pg* phase can be correlated at offsets of 30 to 80 km in the eastern part with an apparent velocity of 5.8 km/s, but is less visible. *PiP* energy is observed beyond 30 km offsets at reduced times of ~5 s to the east, almost a 1 s delay compared to the west. Weak *PcP* arrivals are identified in the eastern section at offsets of 50–90 km, and relatively high amplitude *PmP* arrivals at offsets of 80–190 km. When examined carefully, we identify two arrivals with different slopes. The first event at 80–130 km offset arrives at ~10 s reduced travel time. We identify a second event with velocity greater than 8.0 km/s at 110–140 km and 13–10 s travel times (Figure 3). These two arrivals suggest a complex Moho-topography. We have modeled the two arrivals

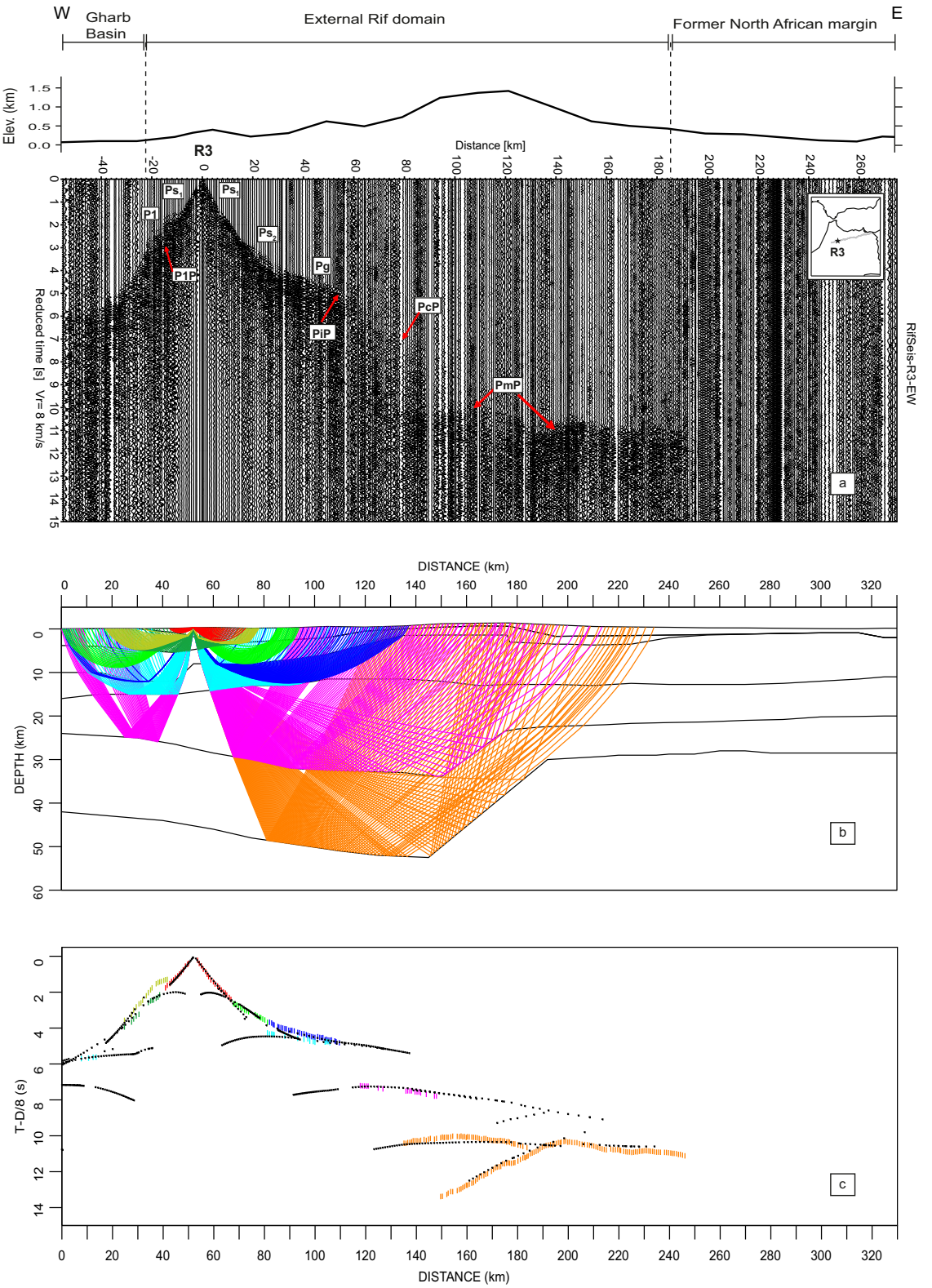

Figure 3. Shot R3 recorded along the EW profile with the ray tracing diagram and the travel time picks considered with topography and geological regions on top. (a) R3 shot record, applying a reduction velocity of 6 km/s and a bandpass filter of 3–10 Hz, showing the quality of the data and the phases identified (see label description in text) and used to build up the seismic velocity model. (b) Ray tracing diagram revealing the extension of the interfaces constrained in the final model. (c) Fitting between travel time picks determined from the data (in colors according to their travel paths) and the ones modeled (in black) by the RAYINVR package [*Zelt and Smith*, 1992]. The vertical bars associated to the travel time picks are indicative of the error estimates considered for each pick. Colors meaning: red: Ps_1 phase; green Ps_2; light green: *P1*; dark green: *P1P*; dark blue: *Pg*; light blue: *PiP*; purple: *PcP*; orange: *PmP*.

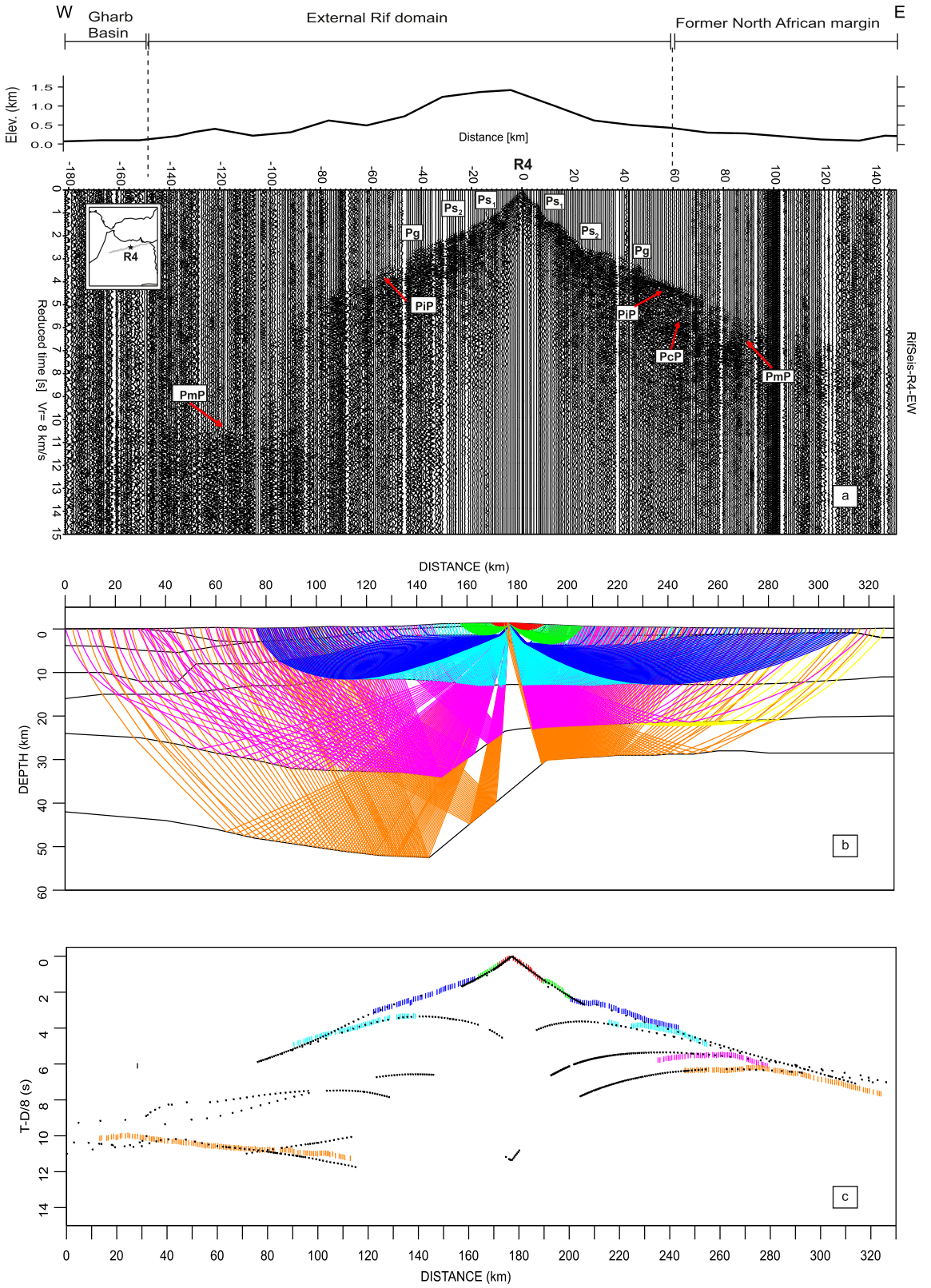

Figure 4. Shot R4 recorded along the EW profile with the ray tracing diagram and the travel time picks considered. See caption in Figure 3 for details.

as different *PmP* branches resulting from a west to east shallowing of the Moho from more than 50 km to less than 30 km. The Moho ramp occurs over a distance of 45–50 km beneath the surface expression of the Nekkor fault/TASZ, at the eastern end of the Bouguer gravity anomaly over the Rif (Figures 1, 2, and 6).

Shot R4, in the center of the EW profile (Figures 1 and 4), clearly exhibits extraordinary lateral differences in crustal structure beneath the Rif resulting from the change in lower crustal structure. Sedimentary phases are observed as first arrivals to 20 km offsets to the west and 30 km to the east, suggesting that the sediments thin from east to west from 4 to 2 km thickness. As will be discussed later, this step in the sediment thickness is located beneath the surface expression of the Nekkor Fault. The velocity in the sedimentary layers increases from 4.3 to 5.3 km/s. The *Pg* phase is visible to 60 km offsets at apparent velocity 5.9 km/s. A reflected event (*PiP*), appearing approximately symmetrically under the shotpoint from 20 to 100 km offset, is interpreted to come from the top of the middle crustal layer at ~16 km depth. To produce the relatively high amplitude of the *PiP* arrivals, a marked velocity contrast is required, which we model as a transition from 5.9 to 6.3 km/s across the interface. Hence, a 10 km thick upper crust is constrained under R4 in contrast with values of 5 km constrained beneath shotpoint R3 (Figure 6).

The *PcP* phase is only observed east of R4 (Figure 4), at around 5.5 s and at offsets of 60 km. Also to the east of R4, following the *PcP* phase we observe a high amplitude *PmP* phase at 6.5 s (Figure 4). The 1 s delay between both phases suggests the presence of a rather thin, ~5 km lower crust to the east of R4. To the east, *PmP* is identified at offsets greater than 70 km to the eastern end of the profile, modeled as a reflection from a Moho at 30 km depth.

The most striking feature in the R4 shot record (Figure 4) is the asymmetry observed in *PmP* across the record section. *PmP* in the west appears from −170 to −60 km offset at reduced travel times of 10–12 s, while in the eastern side it is observed around 7 s. For an offset of 120 km, the difference between the *PmP* phase arrivals at both sides reaches 4 s (Figure 4). This difference is accommodated in the final model by a 20 km difference in crustal thickness (Figures 4 and 6).

Shot record R5 (Figure 5) reveals events from the sedimentary cover, middle crust, lower crust and Moho. In detail a short sedimentary phase is observed to 10 km offset, resulting from a thin (2–4 km) sedimentary layer with a velocity gradient of 3.0 to 3.8 km/s (Figures 5 and 6). The *Pg* phase is correlated to 100 km offset with an average velocity of 6.0 km/s. The *PcP* is visible after 50 km offsets (at about 5 s reduced time at 60 km) and the *PmP* after 60 km offsets, at about 2 s later on, constraining a Moho at the eastern end of the profile at ~29 km depth (see Figures 5 and 6). At offsets between 100 and 250 km, the observed arrivals from the deep crust are fitted in the model (see Figure 5) as corresponding to *PcP* and refracted energy within the lower crust. They could not been attributed to *PmP* to be consistent with the Moho location established after the *PmP* fitting from reverse shot R4 (Figure 4). Hence, the lower crust in the east is 7–8 km thick with a velocity gradient from 6.75 to 6.9 km/s, in strong contrast with the western part of the profile, where the lower crust thickness exceeds 15 km, although its top is poorly resolved from *PcP* phases.

Pn phases that would constrain the upper mantle velocities could not be identified for any of the shots. This is not unusual in areas with significant lateral variations in the crustal thickness, a weak velocity gradient at the uppermost mantle or a smooth crust-mantle transition. However, this latter explanation seems not well in agreement with the short *PmP* critical distances generally observed in our sections. We have fixed an average velocity of 8 km/s in the uppermost mantle and verified that even if this value is not constrained by direct *Pn* observations, a 2–3% modification of the velocity ratio between the lower crust and mantle velocities results in clear misfits between observed and theoretical *PmP* critical distances (supporting information Figure S2).

In summary, in the crustal model along the EW RIFSIS transect (Figure 6) the thickness of sediments is clearly decreasing from west (Gharb Basin) to east (Algerian border). Near R3 up to three sedimentary layers are interpreted in contrast to only one in R5. Upper, middle and lower crustal levels are constrained by refracted and reflected phases (*Pg*, *PiP, PcP* and *PmP*, respectively). The bottom of the crust is well defined from *PmP* phases, although the lack of *Pn* arrivals prevents to constrain upper mantle velocities. A major change in crustal thicknesses can be observed directly in the R4 shot section, which shows differences of 5 s in the *PmP* arrivals at offsets of 120 km. Forward modeling has shown that a rapid change of ~20 km in Moho depth within 50 km horizontal distances is needed to explain these observations. The Moho in this area is sampled in both directions (shots R3 and R4) and hence the final model is here well constrained. Maximum depths around 50 km are found beneath the high topography of the External Rif domain, whereas a thin crust with a 29 km Moho depth is interpreted in the foreland and Atlasic terranes up to the Algerian border.

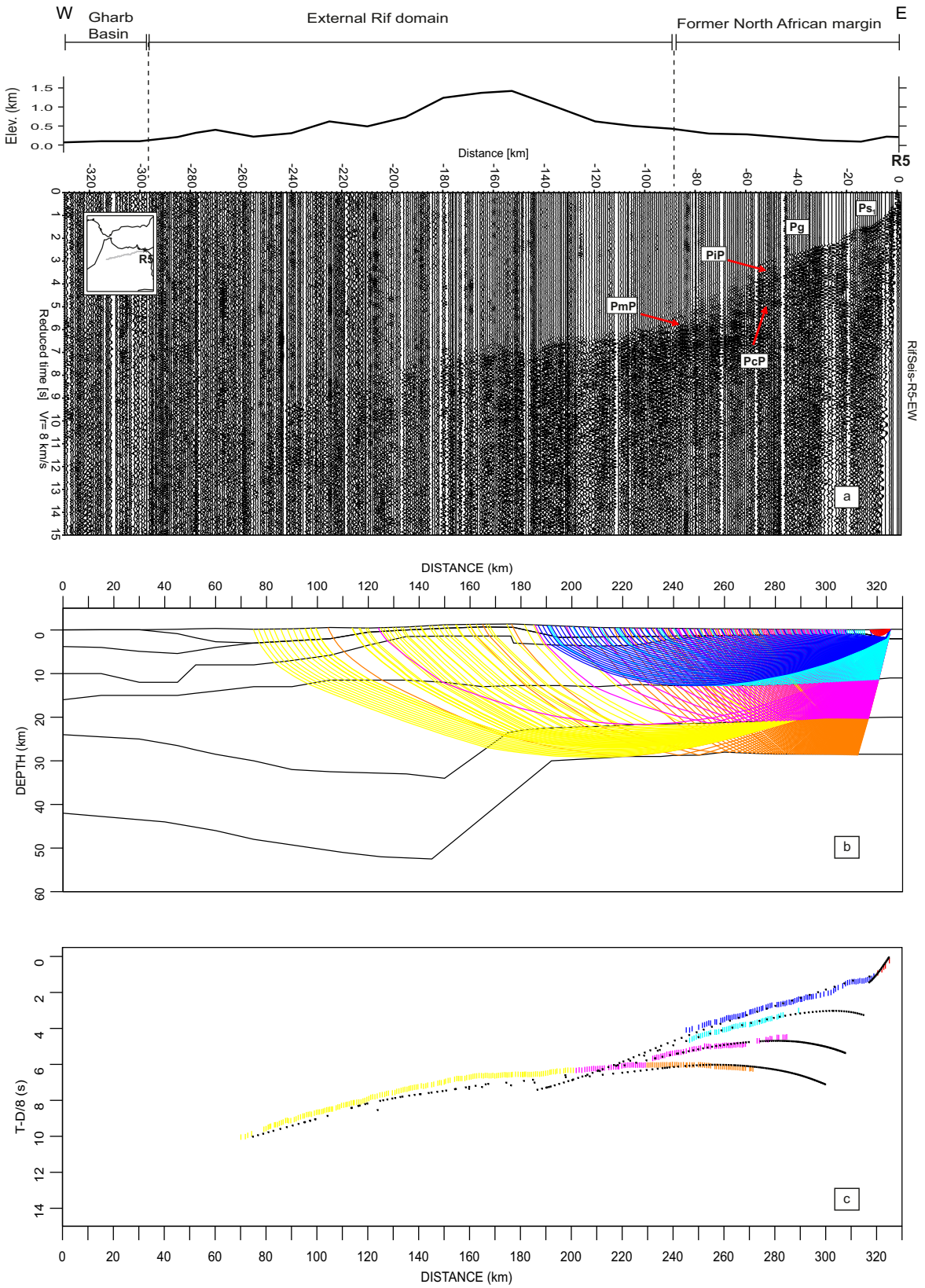

Figure 5. Shot R5 recorded along the EW profile with the ray tracing diagram and the travel time picks considered. See caption in Figure 3 for details.

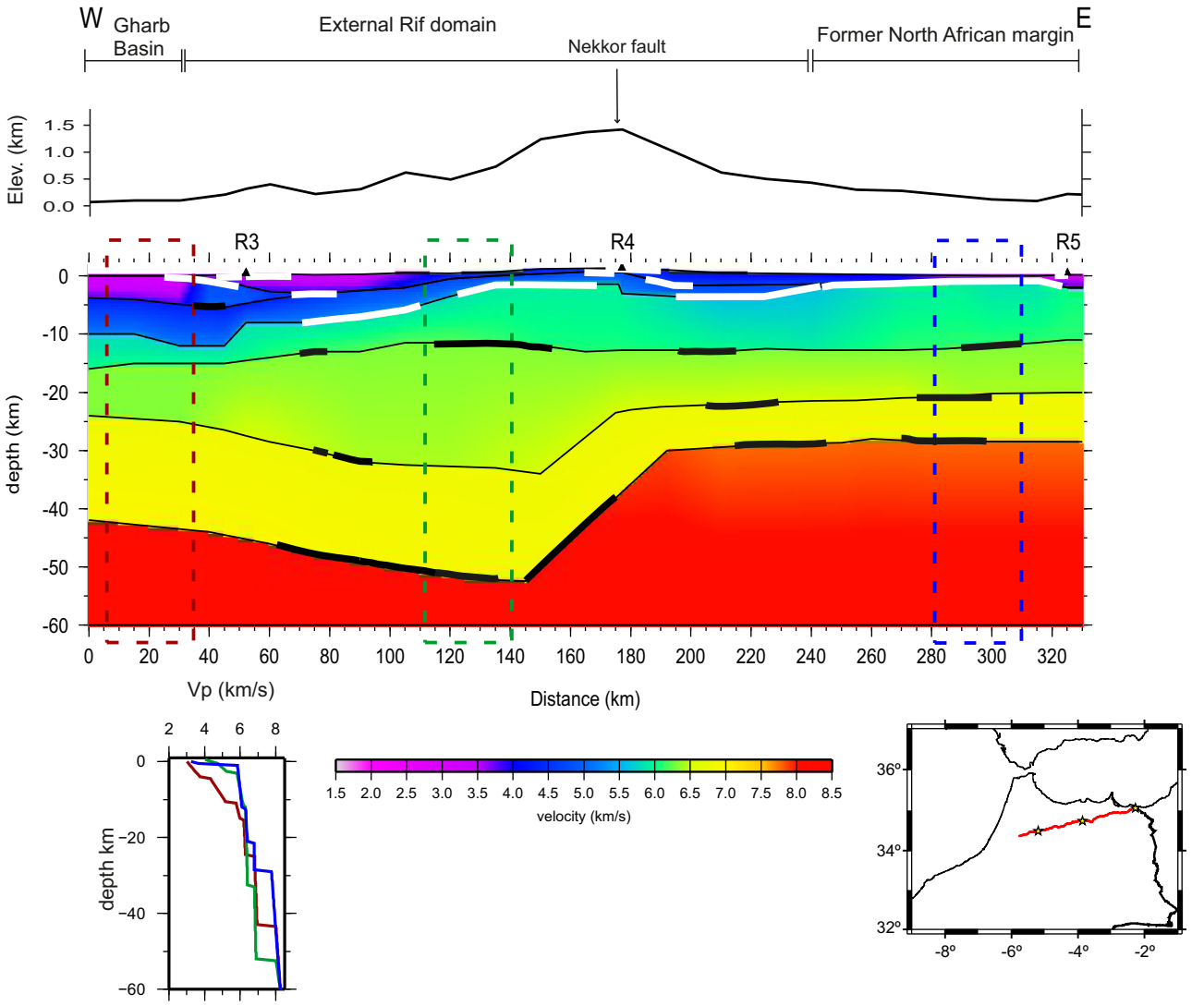

Figure 6. Crustal velocity-depth model determined along the EW profile with a vertical exaggeration of 2:1. The geologic domains are labeled on top of the model, and the topographic profile is sketched. Bold lines indicate layer segments directly sampled by seismic reflections. The vertical rectangles indicate the position where 1-D velocity-depth functions have been estimated, beneath the Gharb Basin (brown), the External Rif domain (green) and the former North African margin (blue).

6. North-South Rif Transect, From Middle Atlas Domains to the Betics Range

The North-South profile crosses the Internal and External Rif domains and the transition to the Middle Atlas in the south and to the Betics in the north. This profile, extending 430 km consisted of three shots, R1–R3 (Figure 1). Shotpoint R3 is at the intersection of the NS and EW transects. Shot R1 was located 6 km south of the Moroccan Mediterranean coast (Figure 1). In Morocco all three shot records show two sedimentary first arrivals: Ps_1 to 10–20 km offset and Ps_2 to 30–40 km (Figures 7–9). North of the Gibraltar strait, the first station on the Iberian Peninsula is located at 35.5 km offset, and no sedimentary waves are visible on R1. Near R1 average velocities for Ps_1 and Ps_2 are 4.0–4.8 km/s with layer thicknesses of 2 and 5 km, respectively (Figures 7b and 10). The *Pg* phase is visible up to offsets of 60 km north and south, with an average velocity of 5.8 km/s and intercept times of 4.5–5 s, probably due to the relatively thick flysch terranes around the shotpoint. The *PiP* phase can be identified from 30 to 80 km in both directions. Low amplitude arrivals characterize the *PcP* phase, identified between 70 and 130 km to the south and between 60 and 80 km to the north. For both *PiP* and *PcP* phases, arrival times are delayed ~1 s to the north relative to the south one, suggesting 5–10 km thickening of the upper-middle crust beneath the Betics relative to the northern Rif (Figure 10). After applying

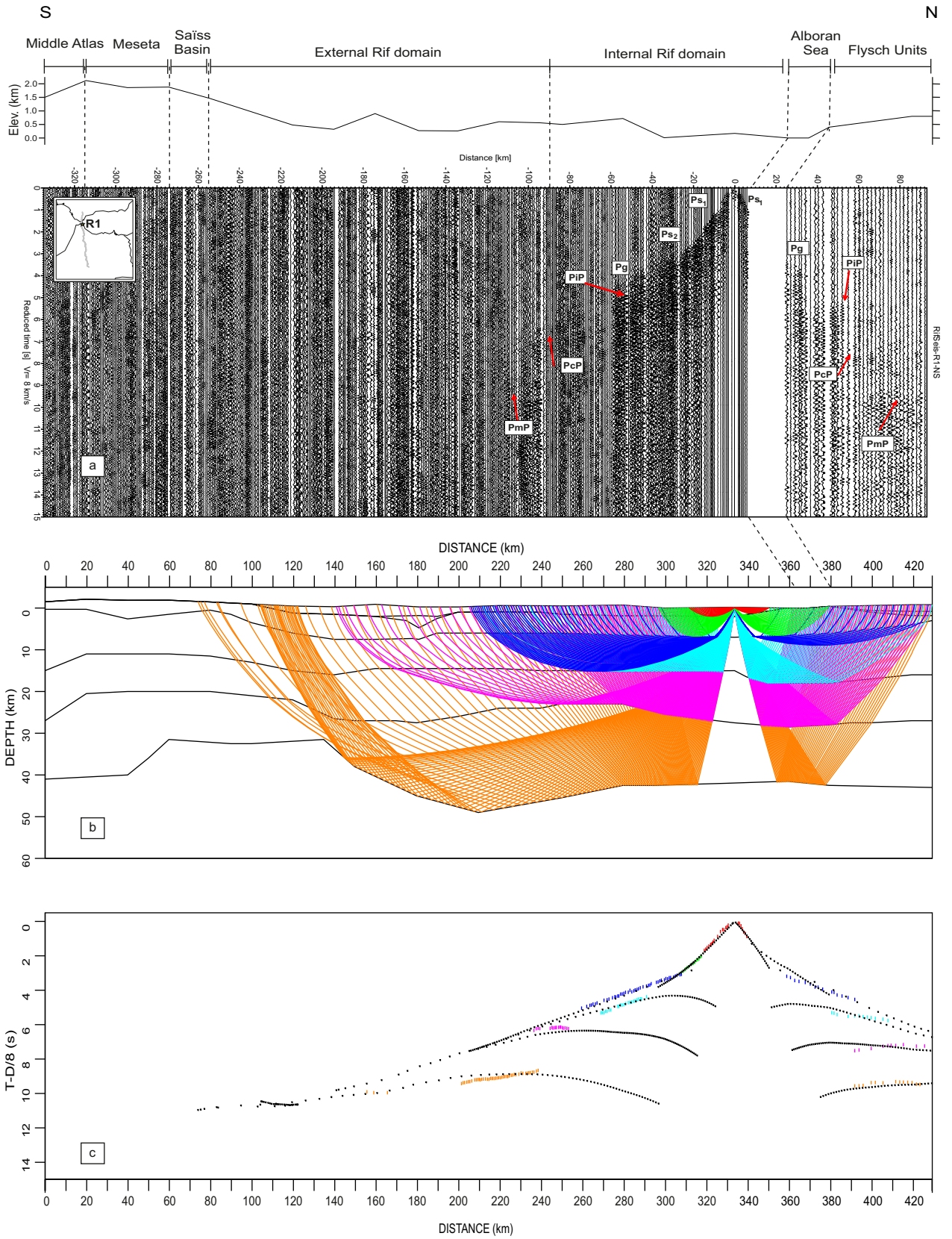

Figure 7. Shot R1 recorded along the NS profile with the ray tracing diagram and the travel time picks considered. See caption in Figure 3 for details.

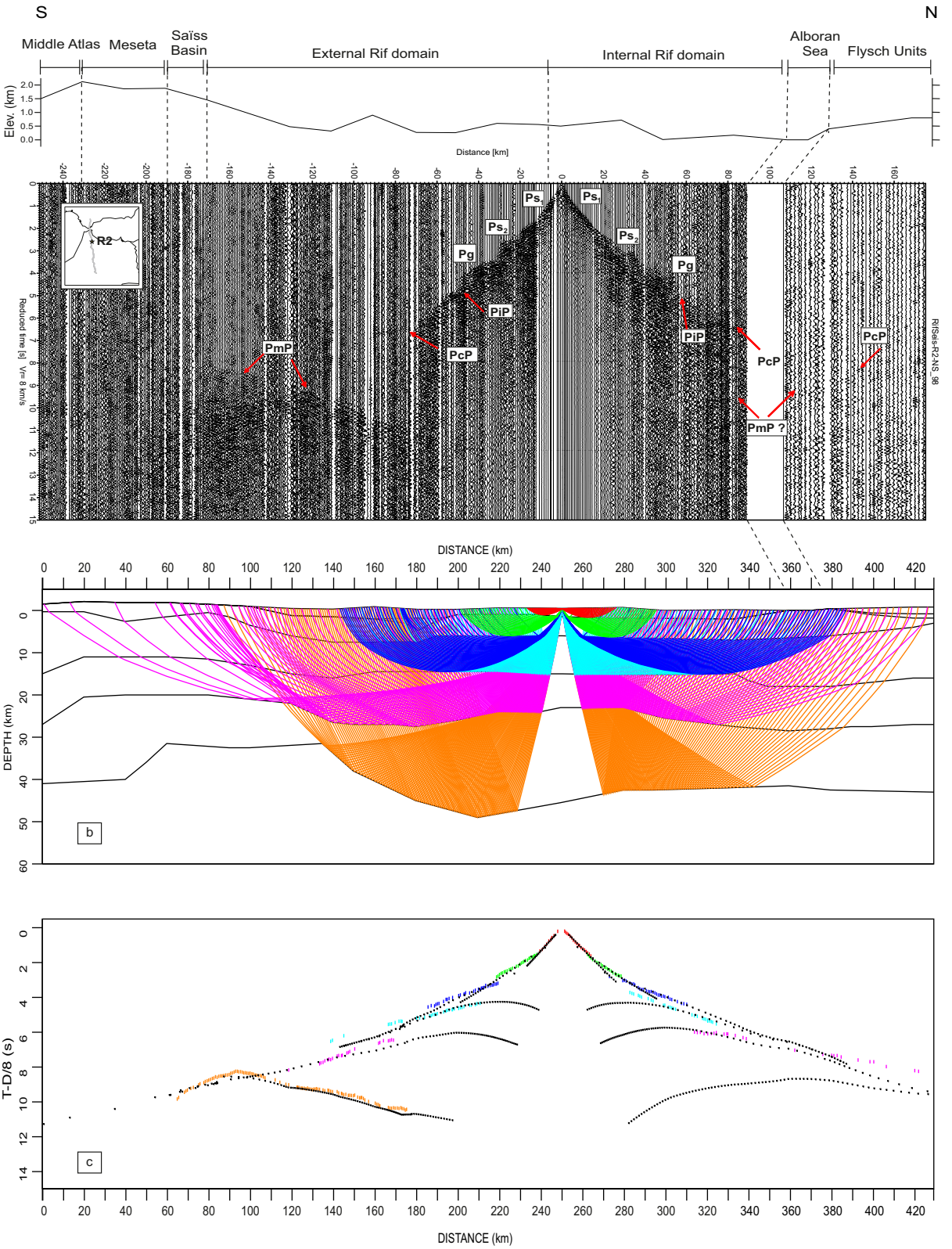

Figure 8. Shot R2 recorded along the NS profile with the ray tracing diagram and the travel time picks considered. See caption in Figure 3 for details.

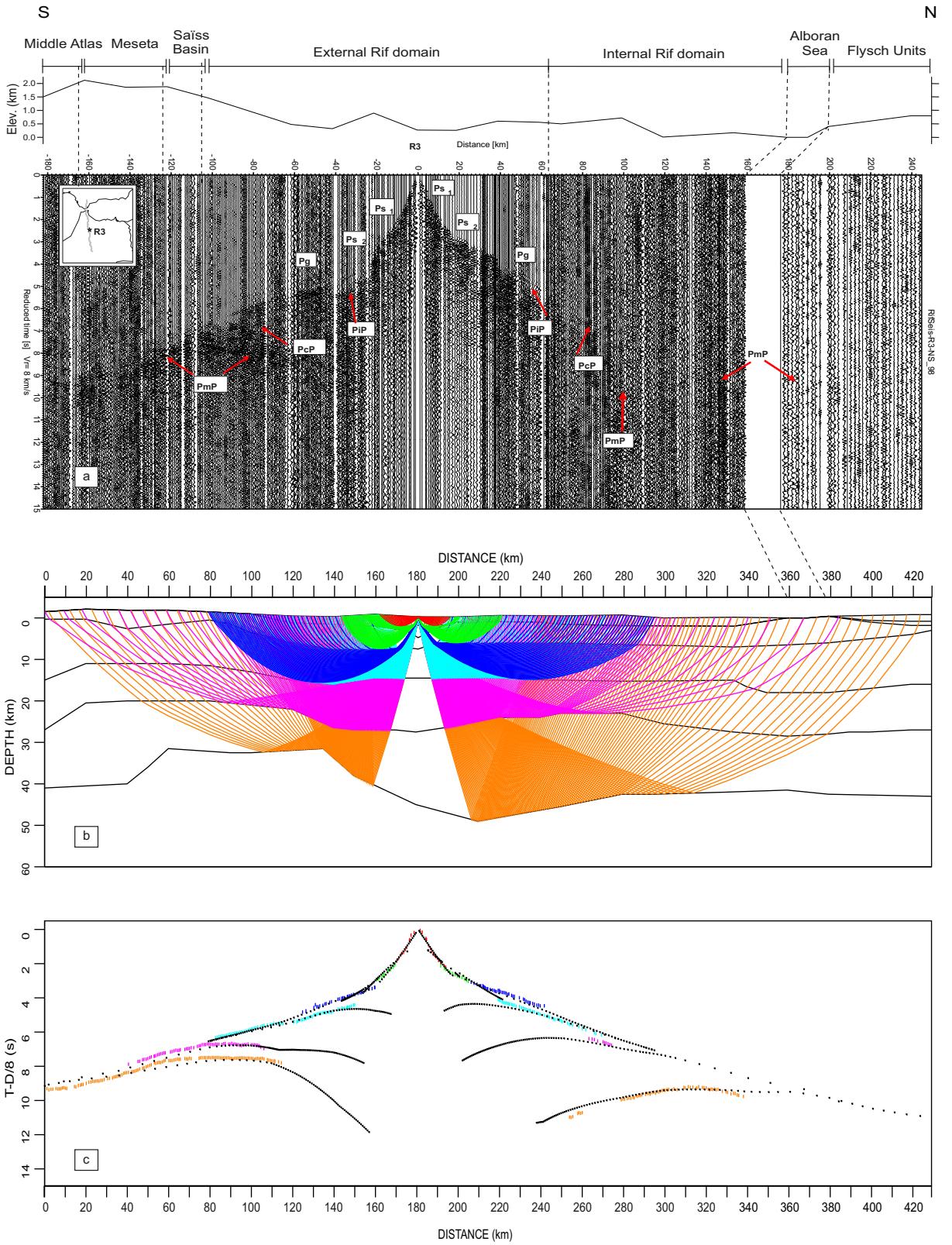

Figure 9. Shot R3 recorded along the NS profile with the ray tracing diagram and the travel time picks considered. See caption in Figure 3 for details.

lateral coherency filtering [*Schimmel and Gallart*, 2007], *PmP* can be identified at offsets between 50 and 140 km to the south, and between 60 and 90 km to the north. Arrival times are approximately the same for the same offset, indicating a rather constant Moho depth, ~42 km, under the area sampled by R1 (Figure 10).

The R2 shotpoint is located ~85 km to the south of R1 (Figure 1). The sedimentary phases, Ps_1 and Ps_2, have velocity values and gradients similar to those at R1. The *Pg* phase is identified to offsets of 80 km with an intercept time of 4.5 s. Intracrustal reflections *PiP* and *PcP* are similar to R1 (Figures 7 and 8). The *PcP* phase is rather weak to the south, in contrast to higher amplitudes to the north to 140 km offset. *PmP* has the highest amplitudes and is identified from 80 to 180 km offset to the south, at reduced times of 11–8 s. *PmP* is not identified to the north.

R3 is located ~155 km from the R1 (Figure 1). As in the other shot records, Ps_1 phases are first arrivals to offsets less than 18 km and are followed by a Ps_2 phase which shows clear differences in apparent velocities north and south (Figure 9). The Ps_2 phase to the north has a higher apparent velocity than the corresponding phase to the south, and to Ps_2 on the other two shots R1 and R2. Shot R3 in the corresponding EW record section indicated a relatively shallow (1.8 km) sedimentary interface separating Ps_1 and Ps_2, giving rise to *P1* and *P1P* in Figure 3. Although these phases are not easily recognized in the NS R3 record section (Figure 9), the marked difference observed in the Ps_2 apparent velocities to the north and south is evidence for the locally limited sedimentary layer from the EW profile.

Pg is clear and can be identified to 90 km offset south, and 60 km offset north (Figure 9). The average apparent velocity is 5.7 km/s with rather large intercept times of 4.5 s north and 5 s south. This constrains the thick Neogene basin below the shotpoint to ~5 km depth. The *PiP* phase appears from 40 to 100 km south, and 30–100 km north, with similar arrival times indicating that the upper crust has a near constant thickness on

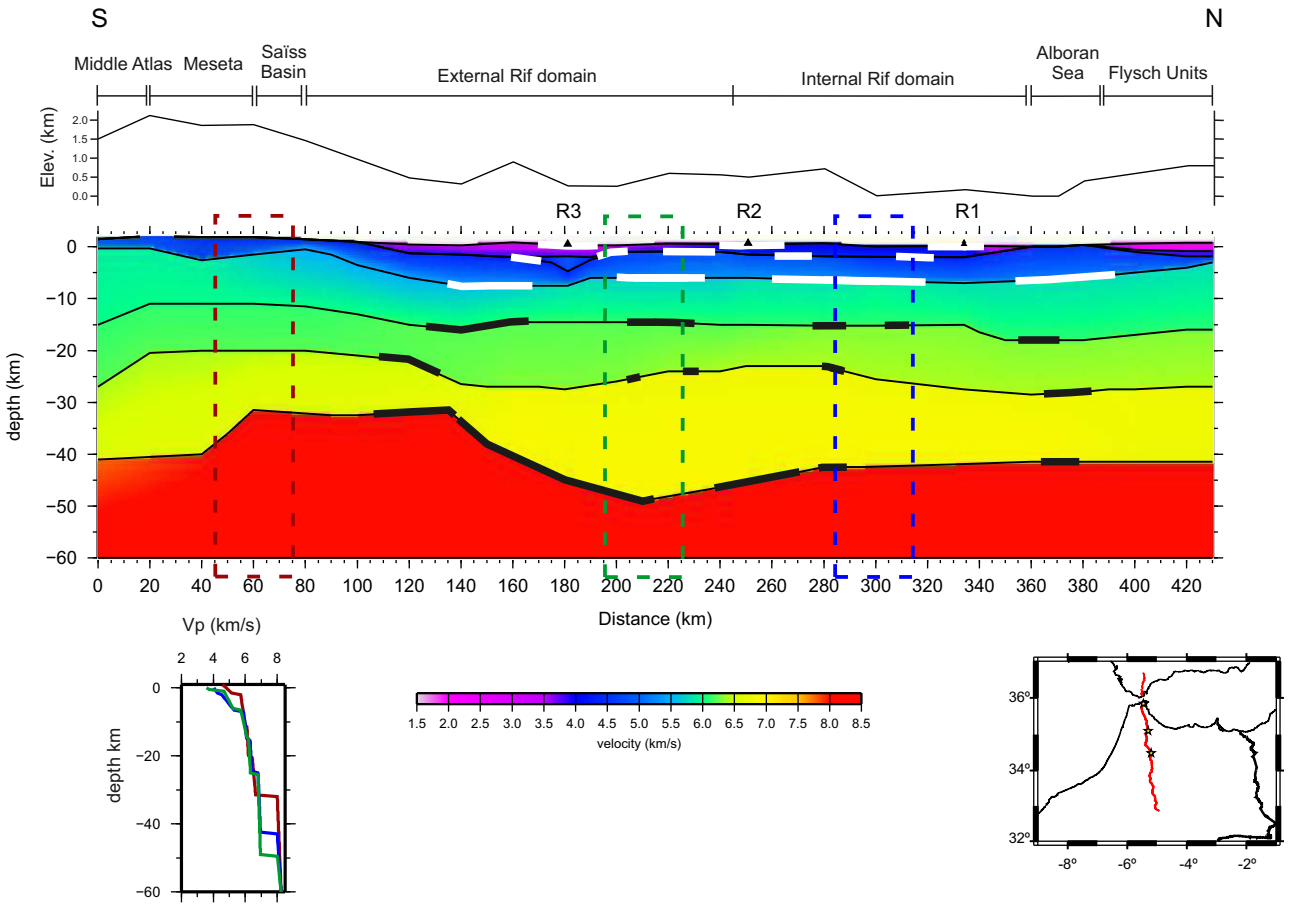

Figure 10. Crustal velocity-depth model determined along the NS profile, with a vertical exaggeration of 2:1. The geologic domains are labeled on top of the model, and the topographic profile is sketched. Bold lines indicate layer segments directly sampled by seismic reflections. The vertical rectangles indicate the position where 1-D velocity-depth functions have been estimated, beneath the Moroccan Meseta (brown), the External Rif domain (green) and the Internal Rif domain (blue).

both side of shotpoint R3 (Figure 9). In the model (Figure 10) the basement is located at 5 km depth, while the bottom of the upper crust is reached at 15 km. The *PcP* phase has been interpreted only to the south (see Figure 9). This phase is observed at offsets of 80–140 km with low amplitude arrivals at 7.5 to 8 s respectively. The base of the crust is constrained by the *PmP* phase, a relatively high amplitude arrival identified at times around 8 s at offsets greater than 70 km south of R3, and with lower amplitudes from 100 to 160 km to the north, at reduced time of ∼9.5 s. The time difference in *PmP* arrivals is evidence of an increase in crustal thickness below R3, with the Moho at ∼47 km depth (Figure 10). This is consistent with the R3 observations along the EW profile (Figure 6). Additional constraints on the southern part of the NS profile are provided by the SIMA project data, a similar wide-angle transect across the High and Middle Atlas that overlapped the NS RIFSIS transect [*Ayarza et al*., 2014]. At the northern end of the profile, in the Betics domain, constraints on the sedimentary structure and upper crust were provided by *Medialdea et al*. [1986].

In summary, the crustal model along the NS RIFSIS transect consists of two sedimentary layers with average velocities of 3.5 and 4.2 km/s inferred from the observed first arrivals (Ps_1, Ps_2 and *Pg*). The upper, middle and lower crusts are constrained by the refracted and reflected phases (*Pg*, *PiP*, *PcP* and *PmP*, respectively). The average velocities within the crust are 5.9, 6.2 and 6.8 km/s. As for the East-West profile we have assumed an 8 km/s velocity below the Moho. Crustal thickness reaches 43 km beneath the Betics and the Internal Rif domain, while under the External Rif sampled area it increases to 47–49 km, with progressive thinning southward into the Middle Atlas where the Moho is found at 31–32 km depth, consistently with the results derived further South by *Ayarza et al*. [2014].

7. Gravity Model

The marked lateral variations in crustal thickness inferred from the seismic models are an outstanding structural feature that can be checked against the corresponding gravity signature. The gravity anomaly beneath the Rif is remarkably low ~ -150 mGal (Figure 2). These Bouguer values are of similar magnitude as those over the Betics and the Atlas, where gravity lows are found over significantly higher elevations. The Rif gravity low is an ellipse slightly shifted to the southwest of the Internal Zones, centered over the External Zones and the western region of the Gharb foredeep basin (Figures 1 and 2). The latter is most likely related to the presence of a large volume (up to 8 km) of continental sediments in the western part of the basin [*Hafid et al*., 2008].

To account for lateral variations perpendicular to the strike of the profiles, gravity data have been averaged over a strip ± 25 km of the profiles with the resulting standard deviation computed and displayed in Figures 11 and 12. The gravity models have been built using the geometry derived from seismic modeling. An averaged P-wave velocity value has been calculated for each layer in the seismic model and the corresponding densities were calculated using the empirical relations by *Brocher* [2005], which applies to most lithologies, except mafic and calcium-rich rocks. The crust is modeled as: sedimentary layers with densities that range from 1800 to 2400 kg/m^3, an underlying crystalline basement with density of 2650 kg/m^3, 2700 kg/m^3 for the upper crust, 2800–2850 kg/m^3 for the middle crust, 2850–2950 kg/m^3 for the lower crust and 3300 kg/m^3 for the uppermost lithospheric mantle. Calculations of the gravity model response are based on the methods of *Talwani et al*. [1959], and *Talwani and Heirtzler* [1964], and the algorithms described in *Won and Bevis* [1987]. The modeled crustal density distribution is well compatible with the P-wave seismic velocity models. To achieve a satisfactory fit to the gravity, the densities in the sedimentary cover needed to be slightly adjusted locally.

For both transects (Figures 11 and 12) the calculated gravity values lie very close to average measurements and well within the standard deviation of the projected gravity estimates. Particular attention has been taken in the segments directly sampled by seismic reflections (thick black lines in Figures 6 and 10) where we have kept the exact geometry as obtained from the velocity model. In all cases the preferred option has been to slightly change the density profile of the crustal layers instead of modifying their geometry. Accordingly, the NS profile (Figure 12) displays lateral density variations at crustal levels from north to south. Densities slightly lower than expected are inferred in the northern segment (from 0 to 140 km), in particular in the lower crust.

8. Discussion

The seismic refraction/wide-angle reflection experiment presented in this P-wave study provides the previously poorly known first order crustal structure of the Rif Mountains in northern Morocco. Crustal interface structure, particularly that of the sedimentary basins and the Moho (Figures 6 and 10) need to be taken into

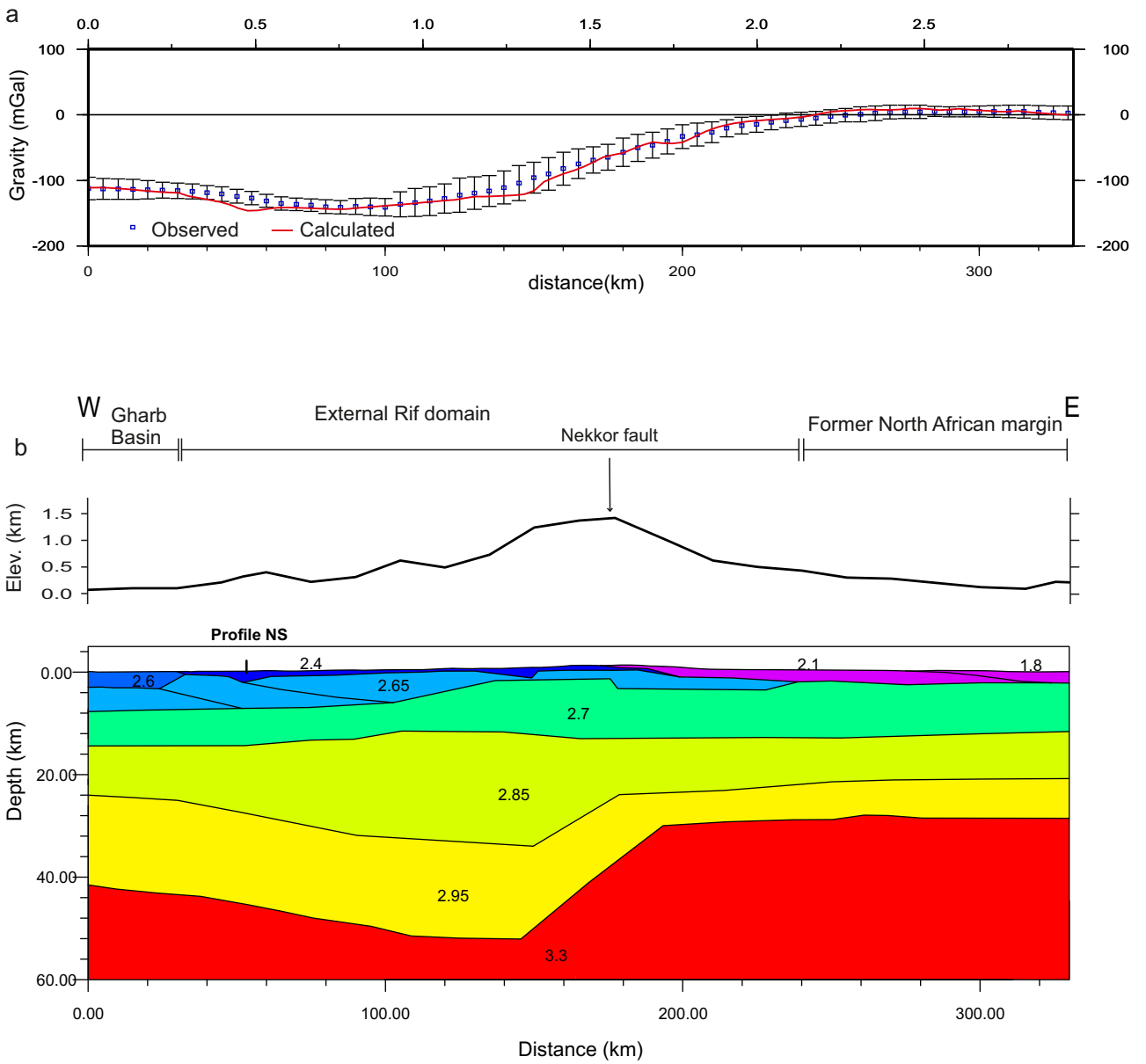

Figure 11. Crustal density model obtained by gravity forward modeling along the EW transect. (a) 2-D projection of the gravity measures extracted from the gravity anomaly map (Figure 2) along a 50 km wide strip. The vertical bars denote standard variation at each measure point, and the red line denote the data fitting with the 2-D gravity profile generated by the density crustal model; (b) distribution of the densities within the crust, inferred from the seismic model (Figure 6). Numbers are density values in (g/cm^3). The geometry for the crustal bodies has been kept and the density structure has been slightly modified to improve the fitting.

consideration in any geodynamic model attempting to address the complex tectonic evolution of the Gibraltar Arc System.

The western end of the EW profile, sampling the Gharb Basin, shows a thick sedimentary cover reaching 10 km. At the transition between the External Rif domain and the Gharb Basin the observation of a fast sedimentary layer westward of shot R3, altogether with the significant change in the total sedimentary thickness, is interpreted as being the deep expression of fold-and-thrust belt, which will reach at least depths around 10 km. This is consistent with previous geological results showing the presence of those structures at an analogue area between the Saïss Basin and the External Rif [*Bargach et al.*, 2004; *Chalouan et al.*, 2006]. Further East, the sedimentary cover thins in a progressive manner to about 2 km near the point at which the Moho is deepest at ~53 km, increases abruptly to 4 km beneath shot R4 and remain 1–3 km thick up to the Algerian border.

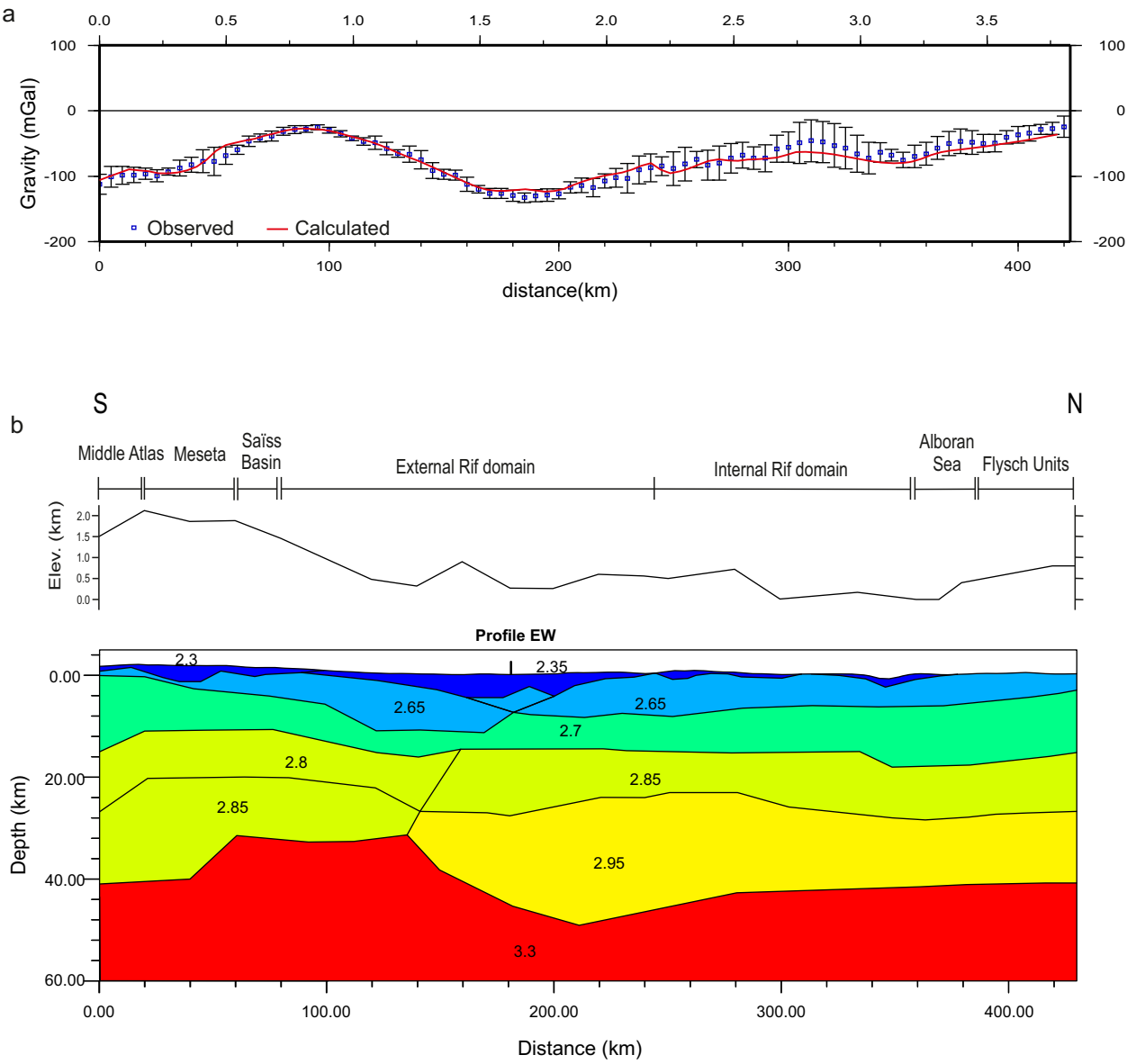

Figure 12. Crustal density model obtained by gravity forward modeling along the NS transect. (a) 2-D projection of the gravity measures extracted from the gravity anomaly map (Figure 2) along a 50 km wide strip. The vertical bars denote standard variation at each measure point, and the red line denote the data fitting with the 2-D gravity profile generated by the density crustal model; (b) distribution of the densities within the crust, inferred from the seismic model (Figure 10). Numbers are density values in (g/cm^3). The geometry for the crustal bodies has been kept and the density structure has been slightly modified to improve the fitting.

From the western end of the profile, the Moho deepens rather smoothly eastward to model coordinate 145 km, where it thins abruptly from 53 km to less than 30 km by 190 km. That is, it decreases around 23 km in thickness over a distance of 40 km. This large and unexpected variation in crustal thickness takes place under the External Rif domain. Farther east, the crustal thickness between model points 190–330 km remains constant, at ∼29 km.

The abrupt change in crustal thickness between 145 and 190 km suggests a tectonic boundary separating two different crustal types, which we attribute to juxtaposition of crustal blocks along the seismically active left-lateral Nekkor strike-slip fault, the onshore continuation of the TASZ. The low shot density and the obliqueness of the profile across the shear zone limits our ability to resolve vertical features. However, a 2 km step in the sedimentary thickness, passing from 4 km eastward of the fault to 2 km westward, has been documented. The Nekkor fault has been active from the late Miocene [*Chalouan et al.*, 2006] and has been linked to the normal faults beneath the Alhoceima region [*Booth-Rea et al.*, 2012]. This region has large

seismic activity in the upper crust, but also moderate seismicity at depths reaching 40 km depth (El Moudnib et al., submitted manuscript), hence suggesting that the Nekkor fault penetrates through the entire crust. The abrupt change in the Moho depth beneath this area depicted by our models strongly supports this hypothesis.

The density model along the EW transect is compatible with the gravity data. Relatively high velocities and densities characterize the root zone. The high *PmP* amplitudes under the root suggest that the Moho is a relatively sharp impedance contrast, as smooth transition will result in changes in the critical distance inconsistent with the data. The lower crust velocities in the southernmost part of the profile are around 6.6 km/s, while beneath the Rif they reach values of 6.8 km/s. This suggests an increase in metamorphic grade of the rocks in the root beneath the Rif. At this point it is difficult to assess the increase of this metamorphic degree, as it could be characteristic of the lower crustal rocks of the Rif crustal domain or it could result from the increased pressures in the crustal root.

Our velocity-depth model evidences a significant mismatch between surface topography and Moho geometry, as the major topographic elevations reaching 1700 m are found around shotpoint R4, coinciding not with the crustal root but with the steep thinning Moho ramp. This effect has previously been observed in active orogens as the Carpathians or the Caucasus and can be explained by an elastic effect, even if other hypothesis, as the presence of mantle mechanisms that contribute to sustain present-day topography cannot be discarded.

Along the NS crustal model the Moho shows also relatively large variations in depth. In the Middle Atlas the Moho is constrained from SIMA wide-angle seismic reflection data [*Ayarza et al*., 2014] and reaches values a little over 40 km depth (Figure 10). The low-density lower crust inferred from the seismic model in this area suggests a mantle contribution to sustain topography. Northward, the Moho shallows to 32 km beneath the northern Meseta and the southern part of the External Rif, then thickens again from model coordinate 140 to 50 km depth at model point 210 km forming the root beneath the northern External Zone of the Rif.

Hence, the most conspicuous structural feature, well constrained from both profiles, is the presence of a 47–53 km thick crust below the External Rif domain, which conforms well to the overall gravity pattern. Moreover, clear lateral variations are observed, particularly a thinning of the crust by ~20 km east of the Nekkor fault. A similar crustal pattern was suggested in recent receiver functions analyses from Topo-Iberia and PICASSO passive seismic surveys [*Mancilla et al*., 2012; *Thurner et al*., 2014], as well as in the velocity anomaly variations inferred from local earthquake tomography and ambient noise data sets (El Moudnib et al., submitted manuscript). GPS observations show that the Rif block is moving S to SW relative to Nubia, with an eastward termination roughly coincident with the Nekkor fault [*Koulali et al*., 2011]. At the lithospheric scale other data sets such as SKS splitting [*Diaz and Gallart*, 2014] and surface wave and teleseismic body wave tomography [*Bezada et al*., 2013; *Palomeras et al*., 2014] also show first order discontinuities below this area. Our results are not consistent with the Moho depth values of 32–36 km previously estimated from heat flow data [*Soto et al*., 2008] or from combining elevation, geoid, gravity and petrological constrains [*Fullea et al*., 2010, 2014].

We emphasized that the Moho depths of ~50 km found below the External Rif domain are significantly greater than those below the Middle or High Atlas and most of the Betic Range [*Ayarza et al*., 2014; *Thurner et al*., 2014]. This increase in crustal thicknesses is accommodated at middle and lower crust levels, while the upper crust has a homogenous thickness of 12–15 km. Our profiles do not provide enough control to discern between a middle or lower crustal thickening (see Figures 6 and 10). Another highlight of these profiles is the existence of a fast sedimentary layer beneath shotpoint R3, the fast layer of 4.8 km/s and double thickness of sediments is likely due to a thrusting, which can be associated to a thrust front and fold axes, similar to what is described by *Bargach et al*. [2004] and *Chalouan et al.* [2006] in the Prerif area.

The complex crustal structure of the Rif domains is a consequence of the Miocene collision between the Iberian and Africa plates combined with the westward rollback of the Neo-Tethys slab. The crustal thinning observed east of the Nekkor fault may be associated with the Neo-Tethys passive margin, the result of Mesozoic rifting [*Gomez et al*., 2000; *Tesón*, 2009]. The crustal thickening under the External Rif can be attributed to slab pull from the downgoing Alboran slab under the Gibraltar Arc System which is imaged in a variety of tomographic images [*Spakman and Wortel*, 2004; *Garcia-Castellanos and Villaseñor* 2011; *Bezada et al*., 2013; *Palomeras et al*., 2014]. However, these interpretations remain open questions to be developed in further investigations.

9. Conclusions

The RIFSIS experiment consists of two wide-angle seismic profiles crossing the Rif Cordillera along NS and EW trends. The 430 km-long NS line extends from the Middle Atlas, across the Rif and Straits of Gibraltar into the Betic Ranges in southern Spain. The 330 km-long EW profile starts at the Gharb Basin and extends to the Morocco-Algeria border. The crustal structure revealed from 2-D forward modeling of the seismic data of both profiles delineates a complex, laterally varying crustal structure that distinguishes the crust of the Rif from surrounding tectonic units.

The velocity-depth models obtained from this experiment image a significant crustal root, with Moho depth reaching 47–53 km beneath the External Rif domain. The crust thins ~20 km over a horizontal distance of 40 km across the Nekkor fault on the EW profile, and over a horizontal distance of 70 km toward the Middle Atlas on the NS profile. This crustal structure identifies a Rif crustal block previously inferred from geodetic data [*Pérouse et al*., 2010]. We interpret this structure as resulting from a complex interaction of the Miocene to present continent-continent collision between Iberia and Africa plates, coupled with slab rollback of the Neo-Tethys Alboran slab.

These results are consistent with the overall Bouguer anomaly pattern, the recent results from receiver function analyses and the velocity anomaly variations inferred from tomographic inversions of local earthquakes, teleseismic body and Rayleigh waves and ambient noise data sets [*Mancilla et al*., 2012; *Palomeras et al*., 2014; *Thurner et al*., 2014; El Moudnib et al., submitted manuscript]. They should prove useful as constraints for future geodynamic modeling on the evolution of the Gibraltar Arc System.

Acknowledgments

This research was funded by Spanish RIFSIS project CGL2009–09727. AG benefited from a PhD grant associated to this project. Support was provided by Spanish projects CSD2006-00041 "Topo-Iberia" and CGL2008–03474 "Topo-Med," as well as the NSF Continental Dynamics Program Grant EAR0808939. We thank many colleagues from the Institut de Ciències de la Terra Jaume Almera (CSIC, Barcelona), Institut Scientifique-Université Mohammed V-Agdal, Rabat, Morocco and Rice University, Texas, US for their help in the field experiment, and Diego Cordoba from the Universidad Complutense de Madrid for providing and managing the Texans instruments deployed in Spain. We also thank Pnina Miller and Mickel Johnson from IRIS-PASSCAL for their processing support, and Bureau Gravimétrique International (BGI)/IAG International Gravity Field Service http://bgi.obs-mip.fr for facilitating the gravity data in the study area. We acknowledge also Puy Ayarza for providing data from SIMA-Atlas experiment and subsequent discussions, Concepción Ayala for her assistance offered in GM-SYS and Jaume Vergés for sharing his knowledge in the Moroccan structural geology. And revision of anonymous reviewers helped to improve the quality of the manuscript. We appreciate the support and technology of ICTJA-CSIC, Barcelona and Rice University, Houston where modeling of these profiles was developed. The data used in this research are available upon request to J. Gallart.

References

Alpert, L. A., M. S. Miller, T. W. Becker, and A. Allam (2013), Structure beneath the Alboran from geodynamic flow models and seismic anisotropy, *J. Geophys. Res.*, *118*, 4265–4277, doi:10.1002/jgrb.50309.

Anahnah, F., et al. (2011a), Crustal resistivity structure of the southwestern transect of the Rif Cordillera (Morocco), *Geochem. Geophys. Geosyst.*, *12*, Q12016, doi:1029/2011GC003783.

Anahnah, F., et al. (2011b),Deep resistivity cross section of the intraplate Atlas Mountains (NW Africa): New evidence of anomalous mantle and related Quaternary volcanism, Tectonics, 30, TC5014, doi:10.1029/2010TC002859.

Ayarza, P., et al. (2014), Crustal thickness and velocity structure across the Moroccan Atlas from long offset wide-angle reflection seismic data: The SIMA experiment, *Geochem. Geophys. Geosyst.*, *15*, 1698–1717, doi:10.1002/2013GC005164.

Bargach, K., P. Ruano, A. Chabli, J. Galindo-Zaldívar, A. Chalouan, A. Jabaloy, M. Akil, M. Ahmamou, C. Sanz de Galdeano, and M. Benmakhlouf (2004), Recent tectonic deformations and stresses in the frontal part of the Rif Cordillera and the Saïss Basin (Fes and Rabat Regions, Morocco), *Pure Appl. Geophys.*, *161*, 521–540, doi:10.007/s00024-003-2461-6.

Bezada, M. J., E. D. Humphreys, D. R. Toomey, M. Harnafi, J. D. Dávila, and J. Gallart (2013), Evidence for slab rollback in westernmost Mediterranean from improved upper mantle imaging, *Earth Planet. Sci. Lett.*, *368*, 51–60, doi:10.1016/j.espl.2013.02.024.

Blanco, M. I. and, W. Spakman (1993), The P wave velocity structure of the mantle below the Iberian Peninsula: Evidence for subducted lithosphere below Spain, *Tectonophysics*, *221*, 13–34, doi:10.1016/0040-1951(93)90025-F.

Booth-Rea, G., A. Jabaloy-Sánchez, A. Azdimousa, L. Asebriy, M. Vazquez-Vilchez, and M. Martínez-Martínez (2012), Upper-crustal extension during oblique collision: The Temsamane extensional detachment (eastern Rif, Morocco), *Terra Nova*, *24*, 505–512, doi:10.1111/j.1365-3121.2012.01089.x.

Brocher, T. A. (2005), Empirical relations between elastic wavespeeds and density in the earth's crust, *Bull. Seismol. Soc. Am.*, *95*, 6, 2081–2092, doi:10.1785/01200050077.

Buontempo, L., G. H. R Bokelmann, G. Barruol and J. Morales (2008), Seismic anisotropy beneath southern Iberia from SKS splitting, *Earth Planet. Sci. Lett.*, *273*, 237–250, doi:10.1016/j.epsl.2008.06.024.

Calvert, A., E. Sandvol, D. Seber, M. Barazangi, S. Roecker, T. Mourabit, F. Vidal, G. Alguacil, and N. Jabour (2000a), Geodynamic evolution of the lithosphere and upper mantle beneath the Alboran region of the western Mediterranean: Constraints from travel times tomography, *J. Geophys. Res.*, *105*, 10,871–10,898.

Calvert, A., E. Sandvol, D. Seber, M. Barazangi, F. Vidal, G. Alguacil, and N. Jabour (2000b), Propagation of regional seismic phases [Lg and Sn] and Pn velocity structure along the Africa–Iberia plate boundary zone: Tectonic implications, *Geophys. J. Int.*, *142*, 384–408.

Carbonell, R., A. Levander, and R. Kind (2013), The Mohorovicic discontinuity beneath the continental crust: An overview of seismic constraints, *Tectonophysics*, *609*, 353–376, doi:10.1016/j.tecto.2013.08.037.

Carbonell, R., P. Ayarza, J. Gallart, J. Diaz, M. Harnafi, A. Levander, and A. Teixell (2014), From the Atlas to the Rif a Crustal seismic image across Morocco: The SIMA & RIFSIS control source wide-angle seismic reflection data, paper presented at EGU General Assembly, Eur. Geosci. Union, Vienna.

Chalouan, A., A. Ouazani-Touhami, L. Mouhir, R. Saji, and M. Benmakhlouf (1995), Les failles normales a faible pendage du Rif interne (Maroc) et leur effet sur l'amincissement crustal du domaine D'Alboran, *Geogaceta*, *17*, 3.

Chalouan, A., A. Michard, H. Feinberg, R. Montigny, and O. Saddiqi (2001), The Rif mountain building (Morocco): A new tectonic scenario, *Bull. Soc. Geol. Fr.*, *172*(5), 603–616.

Chalouan, A., J. Galindo-Zaldívar, M. Akil, A. Chabli, P. Ruano, K. Bargach, C. Sand de Galdeano, M. Benmakhlouf, M. Ahmamou, and L. Gourari (2006), Tectonic wedge escape in the southwestern front of the Rif Cordillera (Morocco), in *Tectonics of the Western Mediterranean and North Africa*, edited by G. Moratti and A. Chalouan, pp. 101–118, Geol. Soc., London, U. K.

Chalouan, A., A. Michard, Kh. El Kadiri, F. Negro, D. Frizon de Lamotte, J. I. Soto, and O. Saddiqi (2008), The Rif Belt, in *Continental Evolution: The Geology of Morocco*, edited by A. Michard et al., pp. 203–302, Springer, Berlin.

Diaz, J., and J. Gallart (2009), Crustal structure beneath the Iberian Peninsula and surrounding waters: A new compilation of deep seismic sounding results, *Phys. Earth Planet. Int.*, *173*, 181–190, doi:10.1016/j.pepi.2008.11.008.

Diaz, J., and J. Gallart (2014), Seismic anisotropy from the Variscan core of Iberia to the Western African Craton: New constrains on upper mantle flow at regional scales, *Earth Planet. Sci. Lett.*, *394*, 48–47, doi:10.1016/j.epsl.2014.03.005.

Diaz, J., J. Gallart, A. Villaseñor, F. Mancilla, A. Pazos, D. Córdoba, J. A. Pulgar, P. Ibarra, and M. Harnafi (2010), Mantle dynamics beneath the Gibraltar Arc (western Mediterranean) from shear-wave splitting measurements on a dense seismic array, *Geophys. Res. Lett.*, *37*, L18304, doi:10.1029/2010GL044201.

Diaz, J., A. Gil, and J. Gallart (2013), Uppermost mantle seismic velocity and anisotropy in the Euro-Mediterranean region from Pn and Sn tomography, *Geophys. J. Int.*, *192*, 310–325, doi:10.1093/gji/ggs016.

Ehsan, S. A., R. Carbonell, P. Ayarza, D. Martí, A. Pérez-Estaún, D. J. Martínez-Poyatos, J. F. Simancas, A. Azor and L. Mansilla (2014), Crustal deformation styles along the reprocessed deep seismic reflection transect of the Central Iberian Zone (Iberian Peninsula), *Tectonophysics*, *621*, 159–174, doi:10.1016/j.tecto.2014.02.014.

Faccenna, C., C. Piromallo, A. Crespo-Blanc, L. Jolivet, and F. Rossetti (2004), Lateral slab deformation and the origin of the Western Mediterranean arcs, *Tectonics 23*, TC1012, doi:10.1029/2002TC001488.

Fadil, A., P. Vernant, S. McClusky, R. Reilinger, F. Gomez, D. B. Sari, T. Mourabit, K. L. Feigl, and M. Barazangi (2006), Active tectonics of the western Mediterranean: GPS evidence for roll back of a delaminated sub-continental lithospheric slab beneath the Rif mountains, *Geology*, *34*, 529–532, doi:10.1130/G22291.1.

Fernàndez, M., X. Berástegui, C. Puig, D. Garcia-Castellanos, M. J. Jurado, M. Torne, and C. Banks (1998), Geophysical and geological constraints on the evolution of the Guadalquivir foreland basin, Spain, in *Cenozoic Foreland Basins of Western Europe*, edited by A. Mascle et al., pp. 29–48, Geol. Soc., London, U. K.

Frizon de Lamotte, D., et al. (2004), TRANSMED transect I Betics, Alboran Sea, Rif, Moroccan Meseta, High Atlas, JbelSaghro, Tindouf Basin, in The TRANSMED Atlas - *The Mediterranean Region from Crust to Mantle*, edited by W. Cavazza et al., pp. 91–96, Springer, Berlin.

Fullea, J., M. Fernàndez, J. C. Afonso, J. Vergés, and H. Zeyen (2010), The structure and evolution of the lithosphere-asthenosphere boundary beneath the Atlantic-Mediterranean Transition Region, *Lithos*, *120*(1-2), 74–95, doi:101016/j.lithos.2010.03.003.

Fullea, J., J. Rodríguez-González, M. Charco, Z. Martinec, A. Negredo, and A. Villaseñor (2014), Perturbing effects of sub-lithospheric mass anomalies in GOCE gravity gradient and other gravity data modelling: Application to the Atlantic-Mediterranean transition zone, *Int. J. Appl. Earth Obs. Geoinf.*, doi:10.1016/j.jag.2014.02.003.

Gallart, J., and J. Diaz (2013), Outstanding Moho depth variations in the Iberian Peninsula, NW Africa and surrounding margins, revealed from controlled-source seismic surveys, paper presented at EGU General Assembly, Eur. Geosci. Union, Vienna.

Garcia-Castellanos, D. (2002), Interplay between lithospheric flexure and river transport foralend basins, *Basin Res.*, *14*(2), 89–104, doi: 10.1046/j.1365-2117.2002.00174.x.

Garcia-Castellanos, D., and A. Villaseñor (2011), Messinian salinity crisis regulated by competing tectonics and erosion at the Gibraltar Arc, *Nature*, *480*, 359–363, doi:10.1038/nature10651.

García-Lobón, J. L., C. Rey-Moral, C. Ayala, L. M. Martín-Parra, J. Matas, and M. I. Reguera (2014), Regional structure of the southern segment of Central Iberian Zone (Spanish Variscan Belt) interpreted from potential field images and 2.5 D modelling of Alcudia gravity transect, *Tectonophysics*, *614*, 185–202, doi:10.1016/j.tecto.2013.12.005.

Gomez, F., W. Beauchamp, and M. Barazangi (2000), Role of the Atlas Mountains (northwest Africa) within the African-Eurassian plate-boundary zone, *Geology*, *28*(9), 775–778, doi:10.1130/0091-7613.

Gómez-Ortiz, D., B. N. P. Agarwal, R. Tejero and J. Ruiz (2011), Crustal structure from gravity signatures in the Iberian Peninsula, *GSA Bull.*, *123*(7/8), 1247–1257, doi:10.1130/B30224.1.

Gurría, E., and J. Mezcua (2000), Seismic tomography of the crust and lithospheric mantle in the Betic Cordillera and Alboran Sea, *Tectonophysics*, *329*, 99–119.

Gutscher, M. A., J. Malod, J. P. Rehault, I. Contrucci, F. Klingelhoefer, L. Mendes-Victor, and W. Spakman (2002), Evidence for active subduction beneath Gibraltar, *Geology*, *30*, 1071–1074.

Hafid, M., G. Tari, D. Bouhadioui, I. El Moussaid, H. Echarfaoui, A. Ait Salem, M. Nahim, and M. Dakki (2008), Atlantic Basins, in *Continental Evolution: The Geology of Morocco*, edited by A. Michard et al., pp. 303–330, Springer, Berlin.

Hatzfeld, D., and D. Bensari (1977), Grands profile sesmiques dans la région de l'arc de Gibraltar, *Bull. Soc. Geol. Fr.*, *7*(XIX-4), pp. 749–756.

Hildenbrand, T. G., R. P. Kucks, M. F. Hamouda, and A. Bellot (1988), Bouguer gravity map and related filtered anomaly maps of Morocco, *U.S. Geol. Surv. Open-File Report*: 88–517, 15 pp.

Jolivet, L., C. Faccenna and C. Piromallo (2009), From mantle to crust: Stretching the Mediterranean, *Earth Planet. Sci. Lett.*, *285*, 198–209, doi:10.1016/j.epsl.2009.06.017.

Koulali, A., D. Ouazar, A. Tahayt, R. W. King, P. Vernant, R. E. Reilinger, S. McClusky, T. Mourabit, J. M. Davila, and N. Amraoui (2011), New GPS constraints on active deformation along the Africa-Iberia plate boundary, *Earth Planet. Sci. Lett.*, *308*, 211–217, doi:10.1016/j.epsl.2011.05.048.

Lonergan, L., and N. White (1997), Origin of the Betic-Rif mountain belt, *Tectonics*, *16*, 504–522, doi:10.1029/96TC03937.

Mancilla, F. L., et al. (2012), Crustal thickness variations in Northern Morocco, *J. Geophys. Res.*, *177*, B02312, doi:10.1029/2011JB008608.

Martínez-Díaz, J. J., E. Masana, J. L. Hernández-Enrile, and P. Santanach (2001), Evidence for coseismic events of recurrent prehistoric deformation along the Alhama de Murcia fault, southern Spain, *Acta Geol. Hipanica*, *36*(3-4), 12.

Martínez-Poyatos, D., et al. (2012), Imaging the crustal structure of the Central Iberian Zone (Variscan Belt): The ALCUDIA Deep seismic reflection transect. *Tectonics*, *31*, TC3017, doi:10.1029/2011TC002995.

Medialdea, T., E. Suriñach, R. Vegas, E. Banda, and J. Ansorge (1986), Crustal structure under the western end of the Betic cordillera (Spain), *Ann. Geophys.*, *4*(B4), 457–464.

Miller, M. S., A. Allam, T. W. Becker, J. F. Di Leo, and J. Wookey (2013), Constraints on the tectonic evolution of the westernmost Mediterranean and northwestern Africa from shear wave splitting analysis, *Earth Planet. Sci. Lett.*, *375*, pp. 234–243, doi:10.1016/j.epsl.2013.05.036.

Palano, M., P. Gonzalez, and J. Fernandez (2013), Strain and stress fields along the Gibraltar Orogenic Arc: Constraints on active geodynamics, *Gondwana Res.*, *23*, 1071–1088, doi:10.1016/j.gr.2012.05.021.

Palomeras, I., S. Thurner, A. Levander, K. Liu, A. Villaseñor, R. Carbonell and M. Harnafi (2014), Finite-frequence Rayleigh wave tomography of the western Mediterranean: Mapping its lithospheric structure, *Geochem. Geophys. Geosyst.*, *15*, 140–160, doi:10.1002/2013GC004861.

Pérouse, E., P. Vernant, J. Chery, R. Reilinger, and S. McClusku (2010), Active surface deformation and sub-lithospheric processes in the western Mediterranean constrained by numerical models, *Geology*, *38*(9), 823–826, doi:10.1130/G30963.1.

Platt, J. P., and R. L. M. Vissers (1989), Extensional collapse of thickened continental lithosphere: An hypothesis for the Alboran Sea and Gibraltar arc, *Geology*, *17*, 540–543.

Platt, J. P., W. M. Behr, K. Johanesen and J. R. Williams (2013), The Betic-Rif Arc and its Orogenic Hinterland: A review, *Annu. Rev. Earth Planet. Sci.*, *41*, 313–357, doi:10.1146/annurev-earth-050212-123951.

Pous, J., et al. (2011), Constraints on the crustal structure of the internal Variscan Belt in SW Europe: A magnetotelluric transect along the eastern part of Central Iberian Zone, Iberian Massif, *J. Geophys. Res.*, *116*, B02103, doi:10.1029/2010JB007538.

Rosenbaum, G., and G. S. Lister (2004), Neogene and Quaternary rollback evolution of the Tyrrhenian Sea, the Apennines, and the Sicilian Maghrebides, *Tectonics*, *23*, TC1013, doi:10.1029/2003TC001518.

Royden, L. H. (1993), Evolution of retreating subduction boundaries formed during continental collision, *Tectonics*, *12*, 629–638, doi: 10.1029/92TC02641.

Ruiz-Constán, A., A. Pedrera, J. Galindo-Zaldívar, J. Pous, J. Arzate, F. J. Roldán-García, C. Marin-Lechado, and F. Anahnah (2012), Constraints on the frontal crustal structure of a continental collision from an integrated geophysical research: The central-western Betic Cordillera (SW Spain), *Geochem. Geophys. Geosyst.*, *13*, Q08012, doi:10.1029/2012GC004153.

Seber, D., M. Barazangi, B. A. Ibenbrahim, and A. Demnati (1996), Geophysical evidence for lithospheric delamination beneath the Alboran Sea and Rif-Betic Mountains, *Nature*, *379*, 785–790, doi:10.1038/379785a0.

Serrano, I., T. M. Hearn, J. Morales and F. Torcal (2005), Seismic anisotropy and velocity structure beneath the southern half of the Iberian Peninsula, *Phys. Earth Planet. Int.*, *150*, 317–330, doi:10.1016/j.pepi.2004.12.003.

Schimmel, M., and J. Gallart (2007), Frequency-dependent phase coherencefor noise suppression in seismic array data, *J. Geophys, Res.*, *112*, B04303, doi:1029/2006JB0046860.

Soto, J. I., F. Fernández-Ibáñez, M. Fernàndez, and A. García-Casco (2008), Thermal structure of the crust in the Gibraltar Arc: Influence on active tectonics in the western Mediterranean, *Geochem. Geophys. Geosyst.*, *9*, 1525–2027, doi:10.1029/2008GC002061.

Spakman, W., and M. J. R. Wortel (2004), A tomographic view on western Mediterranean geodynamics, in *The TRANSMED Atlas—The Mediterranean Region from Crust to Mantle*, edited by P. Ziegler, pp. 31–52, Springer, Berlin.

Talwani, M., and J. R. Heirtzler (1964), Computation of magnetic anomalies caused by two dimensional bodies of arbitrary shape, in *Computers in the mineral industries, Part 1, Geol. Sci. 9*, edited by G. A. Parks, pp. 464–480. Stanford Univ. Publ., Stanford, Calif.

Talwani, M., J. L. Worzel, and M. Landisman (1959), Rapid gravity computations for two dimensional bodies with application to the Mendocino submarine fracture zone, *J. Geophys. Res.*, *64*, 49–59.

Tesón, E. (2009), Estructura y cronología de la deformación en el borde Sur del Alto Atlas de Marruecos a partir del registro tectonosedimentario de la cuenca de antepaís de Ouarzazate, PhD thesis, Univ. Autònoma de Barcelona, Barcelona, Spain.

Thurner, S., I. Palomeras, A. Levander, R. Carbonell and C. T. Lee (2014), Ongoing Lithospheric removal in the Western Mediterranean: Evidence from Ps receiver functions and thermobarometry of Neogene basalts (PICASSO Project), *Geochem. Geophys. Geosyst.*, *15*, 1113–1127, doi:10.002/2013GC005124.

Torne, M., M. Fernàndez, M. C. Comas, and J. I. Soto (2000), Lithospheric structure beneath the Alboran Basin: Results from 3D gravity modeling and tectonic relevance, *J. Geophys. Res.*, *105*, 3209–3228, doi:10.1029/1999JB900281.

Udías, A., and E. Buforn (1992), Sismicidad y sismotectónica de las Beticas, *Física de la Tierra*, *4*, 109–123.

Vergés, J., and M. Fernàndez (2012), Tethys-Atlantic interaction along the Iberia-Africa plate boundary: The Betic-Rif orogenic system, *Tectonophysics*, *579*, 144–172, doi:101016/j.tecto.2012.08.032.

Vernant, P., A. Fadil, T. Mourabit, D. Ouazar, A. Koulali, J. M. Davila, J. Garate, S. McClusky, and R. Reilinger (2010), Geodetic constraints on active tectonics of the Western Mediterranean: Implications for the kinematics and dynamics of the Nubia-Eurasia plate boundary zone, *J. Geodyn.*, *49*, 123–129, doi:10.1016/j.jog.2009.10.007.

Wigger, P., G. Asch, P. Giese, W. D. Heinsohn, S. O. E. Alami, and F. Ramdami (1992), Crustal structure along a traverse across the Middle and High Atlas mountains derived from seismic refraction studies, *Geol. Rundsch.*, *81*(1), 237–248, doi:10.1007/BF01764552.

Wildi, W. (1983), La chaîne tello-rifaine (Algérie, Maroc, Tunisie): Structure, stratigraphie etévolution du Trias au Miocène, Rev. *Dyn. Geogr. Phys.*, *24*, 201–297.

Won, I. J., and M. Bevis (1987). Computing the gravitational and magnetic anomalies due to a polygon: Algorithms and Fortran subroutines, *Geophysics*, *52*, 232–238.

Working Group for Deep Seismic Sounding in Alboran 1974 (1978), Crustal seismic profiles in the Alboran sea-preliminary results, *Pageoph*, *116*, 166–180.

Zeck, H. P. (1996), Betic-Rif orogeny: Subduction of Mesozoic Tethys lithosphere under eastward drifting Iberia, slab detachment shortly before 22 Ma and subsequent uplift and extensional tectonics, *Tectonophysics*, *254*, 1–16, doi:10.1016/0040-1951(95)00206-5.

Zelt, C. A., and R. B. Smith (1992), Seismic traveltime inversion for 2-D crustal velocity structure, *Geophys. J. Int.*, *108*, 16–34, doi:10.1111/j.1365-246x.1992.tb00836.x.

Zeyen, H., P. Ayarza, M. Fernàndez, and A. Rimi (2005), Lithospheric structure under the western African-European plate boundary: A transect across the Atlas Mountains and the Gulf of Cadiz, *Tectonics*, *24*, TC2001, doi:10.1029/2004TC001639.